Relativistic Exact Two-Component Coupled-Cluster Study of Molecular Sensitivity Factors for Nuclear Schiff Moments

Tianxiang Chen,[†] Chaoqun Zhang,[†] Lan Cheng,[*,†] Kia Boon Ng,[*,‡] Stephan Malbrunot-Ettenauer,[‡,∇] Victor V. Flambaum,[¶] Zack Lasner,[*,§] John M. Doyle,[§] Phelan Yu,[⊥] Chandler J. Conn,[⊥] Chi Zhang,[⊥] Nicholas R. Hutzler,[*,⊥] Andrew M. Jayich,[#] Benjamin Augenbraun,[@] and David DeMille[△]

[†]*Department of Chemistry, The Johns Hopkins University, Baltimore, MD 21218, USA*
[‡]*TRIUMF, 4004 Wesbrook Mall, Vancouver, BC V6T 2A3, Canada*
[¶]*School of Physics, University of New South Wales, Sydney 2052, Australia*
[§]*Department of Physics, Harvard University, Cambridge, Massachusetts 02138, USA*
[||]*Harvard-MIT Center for Ultracold Atoms, Cambridge, Massachusetts 02138, USA*
[⊥]*Division of Physics, Mathematics, and Astronomy, California Institute of Technology, Pasadena, CA 91125, USA*
[#]*Department of Physics, University of California, Santa Barbara, California 93106, USA*
[@]*Department of Chemistry, Williams College, 47 Lab Campus Drive Williamstown, MA 01267, USA*
[△]*Department of Physics, University of Chicago, Chicago, Illinois 60637, USA*
[∇]*Department of Physics, University of Toronto, Toronto M5S 1A7, Canada*

E-mail: lcheng24@jhu.edu; kbng@triumf.ca; zlasner@g.harvard.edu; hutzler@caltech.edu

Abstract

Relativistic exact two-component coupled-cluster calculations of molecular sensitivity factors for nuclear Schiff moments (NSMs) are reported. We focus on molecules containing heavy nuclei, especially octupole-deformed nuclei. Analytic relativistic coupled-cluster gradient techniques are used and serve as useful tools for identifying candidate molecules that sensitively probe for physics beyond the Standard Model in the hadronic sector. Notably, these tools enable straightforward "black-box" calculations. Two competing chemical mechanisms that contribute to the NSM are analyzed, illuminating the physics of ligand effects on NSM sensitivity factors.

Introduction

Many open questions in fundamental physics, such as the Baryon Asymmetry[1] and the Strong CP Problem,[2] can be studied using precision measurements of fundamental symmetry violations in atoms and molecules.[3–5] Molecules, in particular, have extreme internal electromagnetic environments which amplify the effects of symmetry-violating electromagnetic moments such as electric dipole moments (EDMs), nuclear magnetic quadrupole moments (MQMs), and nuclear Schiff moments (NSMs) – all of which violate both $T-$ and $P-$ symmetries, and are sensitive to symmetry-violating physics beyond the Standard Model.[6] Sensitivity to nuclear symmetry violations via NSMs can be enhanced by around a thousand-fold in heavy nuclei possessing an octupole (β_3) deformation and non-zero nuclear spin,[7] including statically deformed isotopes of radioactive species Fr, Ra, Ac, Th, and Pa, as well as dynamically deformed isotopes of stable species Eu and Dy, all of which present both experimental and theoretical challenges.

Experiments to search for NSMs using atoms and molecules rely on the symmetry-violating interaction between the nuclear spin and the electronic orbitals by precise comparisons of the energy of two states with opposite nuclear spin orientation.[3] For a given NSM, the induced energy shift, which is the experimental observable, depends on details of

the electronic structure and how the electrons interact with the nucleus. Specifically, the induced energy shift is proportional to a NSM sensitivity factor of the molecular state used in the search.[3] In order to both design and interpret experiments, one needs to calculate this NSM molecular sensitivity parameter by performing quantum-chemical calculations.

Relativistic density functional theory,[8–11] coupled-cluster,[11–14] and mulitreference configuration interaction (MRCI)[15,16] calculations of NSM molecular sensitivity factors have been reported. To improve the robustness and efficiency for calculations with high-level treatments of electron-correlation effects, in this work we extend analytic relativistic coupled-cluster gradient techniques to calculations of NSM molecular sensitivity factors. Molecular structure calculations relevant to experimental searches for NSMs in heavy nuclei, including the exceptionally important case of octupole deformed nuclei, are reported. Further, we analyze two competing chemical mechanisms contributing to the NSM molecular sensitivity parameters and discuss the implication to engineering suitable candidate molecules.

In the following, we first provide general background information about relativistic coupled-cluster theory and precision spectroscopic searches for time-reversal symmetry violation. We then summarize theory and computational details, and present discussions of the computational results. Finally, we provide a summary and an outlook.

Generalities

Coupled-Cluster Theory

Coupled-cluster (CC) methods[17,18] provide size-extensive and systematically improvable treatments of electron correlation in atoms and molecules. The CC singles and doubles (CCSD)[19] method has been shown to capture the majority of electron-correlation effects in electronic states dominated by a single Slater determinant. The inclusion of triple and quadruple excitations in the CC singles doubles triples (CCSDT)[20–22] method and the CC singles doubles triples quadruples (CCSDTQ)[23–26] method paves the way to essentially quan-

titative treatments of electron correlation. More approximate variants, including the CCn models[27,28] and a variety of non-iterative treatments of triple and quadruple excitations,[29–41] improve the computational efficiency compared to the full CCSD, CCSDT, and CCSDTQ models and are useful practical approaches. For example, the CCSD augmented with a non-iterative treatment of triple excitations [CCSD(T)][29–31] method and the CCSDT augmented with a non-iterative treatment of quadruple excitation [CCSDT(Q)][35] method feature balanced computational cost and accuracy and thus are being widely used in molecular calculations. Analytic-derivative formulations for CC methods[42–69] have been developed to enable efficient CC calculations of molecular properties. The availability of analytic CC energy derivatives greatly facilitates chemical and spectroscopic applications of CC methods.

Relativistic effects[70–73] play an important role in heavy-atom-containing molecules, including determining the level structure and measurable consequences of new fundamental particles and forces. For example, the enhancement factors for the electron EDM in atoms[74] and molecules[75] are intrinsically relativistic. Their values may exceed 1,000 when calculated with accurate treatments of relativistic effects, but they vanish in the non-relativistic limit. Relativistic effects also enhance the NSM sensitivity factors in heavy atoms by an order of magnitude.[76] Relativistic CC methods,[77] i.e., CC methods combined with relativistic Hamiltonians, can provide accurate treatments of relativistic and electron-correlation effects for single-reference molecular states containing heavy atoms; they are useful tools for studying heavy-element chemistry and spectroscopy. Scalar-relativistic CC calculations[78–83] retain the spin symmetry and are essentially as efficient as the corresponding non-relativistic CC calculations. On the other hand, relativistic spin-orbit CC (SO-CC) methods[84–91] with variational treatments of spin-orbit coupling, including spinor-based relativistic CC methods, are computationally more expensive because of spin-symmetry breaking. While these methods were most often used in calculations of atoms and small molecules, recent algorithmic and implementational advances extend the applicability of SO-CC methods to larger molecules.[77,91–93]

Atoms and Molecules as Probes for New Physics

Precision searches for energy-level splittings due to time-reversal symmetry-violating interactions provide a promising approach to search for undiscovered fundamental physics beyond the Standard Model (BSM).[3,94–96] In particular, heavy-atom-containing polar molecules possess orders of magnitude larger time-reversal symmetry-violating sensitivity parameters compared to atoms due to their ability to be polarized in lab fields;[3] such molecules can serve as sensitive probes of BSM physics.[97,98] As a prominent example, the use of molecules in searches for the electron's electric dipole moment (eEDM) has improved the upper bound for the eEDM value by several orders of magnitude[99–104] compared to the earlier record obtained from atoms.[105] The ongoing work on improving existing experiments aims at orders of magnitude further improvement.[106–110] The EDM experiments may also be used to search for $P - T$ violating interactions between electrons and nucleons in atoms and molecules mediated by new fundamental particles such as the axion, which is one of the leading candidates for dark matter and was originally proposed to solve the strong CP problem.[111–119]

The targeted interactions in the precision spectroscopy searches of new physics are related to intrinsic electronic-structure properties of atoms and molecules, which can only be obtained from first-principle calculations until symmetry violations are observed. For example, the searches for the eEDM in atoms and molecules probe an energy shift that scales with both the eEDM–an intrinsic property of the electron–and a sensitivity parameter known as the "effective electric field"[3,74,75,120,121] that depends on the atomic or molecular state used in the search, often referred to as the "science state." First-principle calculations for sensitivity parameters of the science states play an essential role in selecting candidate molecules and in interpreting measurement results.

Science states of atoms and molecules in the precision measurement searches for BSM physics often comprise single-reference electronic states, i.e., electronic states dominated by a single electron configuration, since their relatively simple structure makes them attractive candidates for experiments. For example, among the science states being used in

eEDM searches, the $X^2\Sigma$ state of YbF is dominated by a $\text{Yb}^+[6s^1]\text{F}^-$ configuration, the $^3\Delta_1$ states of ThO and ThF^+ are dominated by a $\text{Th}^{2+}[7s^16d^1]\text{O}^{2-}$ configuration and a $\text{Th}^{2+}[7s^16d^1]\text{F}^-$ configuration, respectively, and the $^3\Delta_1$ state of HfF^+ is dominated by a $\text{Hf}^{2+}[6s^15d^1]\text{F}^-$ configuration. Spinor-based relativistic coupled-cluster methods have served as important tools to provide accurate computed properties, e.g., the effective electric field,for these states.[107,108,122–131]

The campaign to observe BSM physics in general calls for a broad search for time-reversal symmetry-violating interactions including effects in both the leptonic and hadronic sectors.[3] In addition to the eEDM, atomic and molecular systems with a nuclear spin $I > 0$ can exhibit T-violating energy shifts arising from the NSM, and systems with $I > 1/2$ can exhibit T-violating shifts arising from the nuclear MQM (NMQM). Each nuclide of the appropriate spin possesses its own characteristic NSM and NMQM values, which can arise from a combination of many underlying T-violating parameters including quark EDMs, quark chromo-EDMs, pion-nucleon couplings, and the Standard Model θ_{QCD} parameters.[132,133] For spherical nuclei, NSMs involve contributions from both valence and internal nucleons,[134] whereas NMQM values are dominated by the valence nucleon.[133] Mechanisms exist to enhance both parameters in deformed nuclei. Quadrupole deformed nuclei exhibit NMQMs enhanced by 1–2 orders of magnitude because many nucleons can occupy open shells.[133,135,136] Octupole deformation leads to additional mechanisms that increase the NMQM by ∼1 order of magnitude compared to spherical nuclei[137] and the NSM by ∼1–3 orders of magnitude[76,132,138,139] due to symmetry-violating-interactions that mix the ground and nearly degenerate excited nuclear states. An axion dark matter field may also produce oscillating NSMs and NMQMs.[140–142] There is growing interest in measurements of both NSMs and NMQMs.[7,143–149] In this vein, an important application of spinor-based relativistic CC methods is the prediction of time-reversal symmetry-violating sensitivity parameters in atoms and molecules for probes of new physics beyond the Standard Model (BSM).[11–16,123,125,126,128–131,146,150–176]

Molecular Structure Calculations Relevant to NSMs

In this work, using analytic relativistic coupled-cluster gradient techniques, we perform molecular structure calculations relevant to experimental searches for NSMs in heavy nuclei, including the exceptionally important case of octupole deformed nuclei. Polar molecules are sensitive probes of the NSMs in their constituent nuclei.[177] As described in detail in the theory section, an NSM produces an energy shift in an atom or molecule that scales with the electron density gradient near the nucleus. A nonzero density gradient at the nucleus is primarily present in $s - p$ hybridized wave functions. While an electron density gradient can be achieved in atoms by polarizing electronic orbitals in an external electric field, in practice only modest density gradients at a nucleus can be experimentally achieved due to the infeasibly large applied electric fields that are required for full polarization. On the other hand, electronic orbitals in polar molecules naturally exhibit large density gradients at heavy atomic nuclei, and the molecules must only be oriented in the lab frame in order to provide full access to the NSM interaction. The ratio of the T-violating energy shift of a fully oriented molecule and the corresponding NSM is referred to as the "molecular sensitivity factor." Note that the overall sensitivity of a molecular species to BSM physics relies on understanding both the molecular sensitivity factor, which is discussed in this work, and the nuclear sensitivity factor, which is not.[5]

Such a molecular sensitivity factor for the NSM interaction in a polar molecule is an intrinsic electronic-structure property and at the present stage can only be obtained from electronic-structure calculations. In the relativistic CC[11–14] and MRCI[15,16] calculations reported previously, these parameters have been calculated as first derivatives of electronic energies using numerical differentiation of electronic energies[11–13] or approximate analytic-gradient formulations.[14–16] These calculations are challenging because of the high computational cost of spinor-based relativistic CC and MRCI methods. In addition, since the NSM sensitivity factor probes the derivative of the electron density distribution in the vicinity of a heavy atom, tedious numerical differentiation procedures are required to ensure numerical

stability in the finite-difference procedure.

The evaluation of NSM sensitivity factors as analytic relativistic coupled-cluster energy gradients is a promising scheme to expedite the calculations. An analytic coupled-cluster gradient calculation is around 2-3 times as expensive as a corresponding energy calculation[58] and can provide all first-order properties including various symmetry-violation sensitivity parameters. It is also free from the complication of the numerical-differentiation procedure and hence is of a "black-box" nature. We have recently developed analytic gradients for exact two-component (X2C) CCSD, CCSD(T), and equation-of-motion CCSD (EOM-CCSD) methods.[178–180] We have demonstrated calculations of effective electric fields based on analytic X2C-CCSD and CCSD(T) gradient techniques.[172] In this work, we extend the applicability to calculations of NSM molecular sensitivity factors, aiming to transform these previously complicated calculations into routine applications of a black-box nature.

Theory and Computational Details

The contribution from the nuclear Schiff moment (NSM) interaction to the molecular energy is given by[177]

$$E_{\text{NSM}} = \frac{3ke}{B} \langle \Psi | S_z \sum_j (z_j - z_N) \rho_N(\vec{r}_j; \vec{r}_N) | \Psi \rangle, \tag{1}$$

in which $|\Psi\rangle$ is the molecular wave function, S_z is the component of the NSM along the molecular axis, $\rho_N(\vec{r}; \vec{r}_N)$ is the nuclear charge density at $\vec{r}$ of the active nucleus centered at $\vec{r}_N$, and $\vec{r}_j$ represents the position of electron j. The constant B is a property of the nuclear distribution, described below. In the following we adopt the natural units of $k = e = 1$, where k is Coulomb's constant and e is the elementary charge. The expression above can be interpreted as the electrostatic interaction between the electrons and an electric field approximately along the $\text{sgn}(S_z)\hat{z}$ direction within the nucleus.[181]

In our calculations we adopt a finite nuclear model using a single Gaussian function

to represent the nuclear charge distribution. Within this model, a finite nuclear charge distribution for nuclear charge Z with a radial distribution of a Gaussian function

$$\rho_N(r) = \rho_0 e^{-\xi r^2} \; , \; \rho_0 = Z \left(\frac{\xi}{\pi}\right)^{3/2} \tag{2}$$

centered at $\vec{r}_N$ can be written as

$$\rho_N(\vec{r}; \vec{r}_N) = \rho_0 e^{-\xi(\vec{r}-\vec{r}_N)^2}. \tag{3}$$

B is defined as

$$B = \int_0^\infty \rho_N(r) r^4 dr, \tag{4}$$

and takes the simple form[16]

$$B = \frac{3}{8\pi\xi} \tag{5}$$

when this Gaussian nuclear distribution is used.

The effective Hamiltonian for the NSM interaction can thus be written as

$$\hat{H}_{\text{NSM}}^{\text{eff}} = S_z W_{\text{NSM}}, \tag{6}$$

with the NSM sensitivity factor W_{NSM} defined as

$$W_{\text{NSM}} = \frac{3}{B}\langle\Psi| \sum_j (z_j - z_N)\rho_N(\vec{r}_j; \vec{r}_N)|\Psi\rangle. \tag{7}$$

Equivalently, for the nuclear density described by Eq. 3, W_{NSM} can be written in terms of the first derivative of the "effective density" with respect to the coordinate of the center of

9

the nuclear charge distribution

$$W_{\text{NSM}} = 4\pi \left.\frac{\partial \bar{\rho}_e[\vec{r}_C]}{\partial z_C}\right|_{\vec{r}_C = \vec{r}_N}, \tag{8}$$

in which the effective density, $\bar{\rho}_e[\vec{r}_C]$, at a position $\vec{r}_C$ is defined in the same way as in the calculations of isomer shifts in Mössbauer spectroscopy,[182,183]

$$\bar{\rho}_e[\vec{r}_C] = \langle\Psi| \sum_j \rho_N(\vec{r}_j; \vec{r}_C)|\Psi\rangle. \tag{9}$$

In the present calculations the origin of the coordinate system is chosen as the center of mass of a molecule. The coordinates of the active nucleus always assume positive values, namely, $z_N > 0$. Therefore, a negative (positive) value for W_{NSM} represents excessive (deficient) effective electron density in the inter-atomic bonding region.

As shown in Eq. (7), W_{NSM} is an expectation value of the molecular wave function. It can be evaluated as the first derivative of the electronic energy by augmenting the molecular Hamiltonian $\hat{H}_0$ with the NSM interaction $S_z\hat{H}_{\text{NSM}}$

$$\hat{H} = \hat{H}_0 + S_z\hat{H}_{\text{NSM}}, \ \ \hat{H}_{\text{NSM}} = \frac{3}{B}\sum_j (z_j - z_N)\rho_N(\vec{r}_j; \vec{r}_N), \tag{10}$$

and evaluating the first derivative of the electronic energy with respect to S_z, namely,

$$W_{\text{NSM}} = \left.\frac{\partial E}{\partial S_z}\right|_{S_z=0}. \tag{11}$$

Within the analytic relativistic coupled-cluster gradient formulation, W_{NSM} is evaluated in a straightforward manner by contracting the relaxed coupled-cluster one-electron density matrix with one-electron integrals for $\hat{H}_{\text{NSM}}$. This avoids the complication in numerical differentiation and enables black-box calculations of this parameter.

The calculation of W_{NSM} has been implemented in the CFOUR program package[184,185] us-

ing the analytic-gradient implementation for exact-two-component (X2C) CCSD and CCSD(T) methods.[178] We have used the analytic X2C-CC gradient module developed earlier to calculate the relaxed X2C-CCSD and CCSD(T) one-electron density matrices and to construct X2C derivative integrals[82] from four-component property integrals. The new implementation work is focused on the evaluation of the four-component integrals for the operator $\hat{H}_{NSM}$. To ensure numerical stability, quadruple precision has been adopted in the evaluation of these integrals. The correctness of this implementation has been verified in two ways. First, since $\sum_j \rho_N(\vec{r}_j; \vec{r}_N)$ is involved in the calculations of effective densities in Mössbauer spectroscopy, we have verified the correctness for the evaluation of four-component integrals for $\sum_j \rho_N(\vec{r}_j; \vec{r}_N)$ by comparing the computed effective densities to reference values in the literature.[183] Then the multiplication with $z_j - z_N$ is straightforward to add in the program module to obtain integrals for W_{NSM}. Second, we perform numerical differentiation of effective densities to obtain W_{NSM} values based on Eq. (8) and compare the results to W_{NSM} values obtained as analytic energy derivatives. In the finite-difference procedure, we calculate effective densities on nine grid points [$\vec{r}_C - \vec{r}_N$=(0, 0, $n \times 10^{-8}$), n=-4, -3, $\cdots$, 3, 4] relative to the active nucleus. We fit the results to a fourth-order polynomial to extract the first derivative of the effective density with respect to the coordinate and then convert it into W_{NSM} using Eq. (8). The W_{NSM} values thus obtained via numerical differentiation agree well with the values obtained from the analytic evaluation, with discrepancies below 0.02%.

All of the calculations presented here have used the X2C Hamiltonian[186–188] with atomic mean-field integrals[189] (the X2CAMF scheme)[190,191] to treat relativistic effects. Gaussian nuclear distributions as parametrized in Ref.[192] have been used throughout the calculations. We have adopted the X2CAMF scheme based on the Dirac-Coulomb-Breit Hamiltonian[191] in the calculations, except that we have performed one calculation using the X2CAMF scheme based on the Dirac-Coulomb Hamiltonian [the X2CAMF(DC) scheme][190] for comparison to a four-component DC calculation. The spinor-based X2CAMF-CC calculations have been

expedited using the recent implementation of atomic-orbital based algorithms.[91] The CC calculations have correlated the valence and semicore electrons defined in the supporting information.

Since the NSM sensitivity factor probes the electron-density gradient in the vicinity of a heavy nucleus, an accurate calculation requires the basis sets to describe the wave functions close to the nucleus with high accuracy. Standard basis sets optimized for chemical properties are insufficient for this purpose; even the uncontracted versions of standard basis sets have been shown to exhibit instability in calculations.[15] The present study has employed even-tempered series of s- and p-type functions for the targeted atoms to ensure a unified description for core and valence regions. A general scheme to construct basis sets is to take the uncontracted version of a standard basis set and replace the portion of s- and p-type functions exhibiting exponent intervals larger than 2.5 with even-tempered basis (ETB) sets with exponents given by $\{\alpha\beta^{m-1}, m = 1, \cdots, n\}$, in which $\beta = 2.5$, and ensure that the largest exponent in the ETB series is greater than 10^8 to obtain a good description of the core region. We have used basis sets of triple-zeta quality in this procedure to obtain the "ETB0" sets. For example, the ETB0 set for thorium is obtained by taking the uncontracted ANO-RCC basis set[193,194] and replacing the s-type functions having exponents larger than 78732.668 with an even-tempered series with exponents $\{\alpha\beta^{m-1}, \alpha = 78732.668, \beta = 2.5, m = 2, \cdots, 9\}$ and p-type functions having exponents larger than 4672.81862 with an even-tempered series with exponents $\{\alpha\beta^{m-1}, \alpha = 4672.81862, \beta = 2.5, m = 2, \cdots, 12\}$. The ETB0 sets have been used in most of the calculations presented here. In order to study the remaining basis-set effects beyond the ETB0 sets, we have carried out calculations using basis sets with additional tight functions and high angular momentum functions. The basis sets and molecular structures used in the present calculations are documented in the Supporting Information.

Results and discussions

Benchmark studies: Basis-set convergence, electron-correlation contributions, and comparison with literature

Let us first study the dependence of the computed NSM sensitivity factors (the W_{NSM} values) to the choice of basis sets. We start with a study of the contributions from additional tight s- and p-type functions. We add three additional tight s- and p-type functions to the ETB0 sets to obtain the ETB0+SP3 sets. As shown in Table 1, the inclusion of three additional tight s- and p-type functions makes small contributions to the computed W_{NSM} values. In the case of FrLi, the difference between ETB0+3SP and ETB0 results amounts to -60 a.u. at the HF level, less than 0.03% of the total value, and 2 a.u. in the electron-correlation contribution (W_{NSM} is presented in atomic units of $E_h(ea_0^3)^{-1}$ throughout). The corresponding contributions in RaF and ThO are also insignificant. Therefore, the ETB0 sets have sufficient tight s- and p-type functions for accurate calculations of the NSM sensitivity factors. We then investigate the use of even-tempered d-type functions in the calculations. We replace the d-type functions in the ETB0 sets with even-temper sets of d-type functions to obtain the ETBSPD sets. The differences between ETBSPD and ETB0 results amount to 0.04% of the total value in the case of FrLi and around 1% for RaF and ThO. They appear to be insignificant compared with other sources of errors, e.g., the electron-correlation contributions; it is thus sufficient to use the d-type functions in the standard basis sets for the calculations of W_{NSM}. Finally, we include higher angular momentum functions to enhance the quality of the basis sets to quadruple-zeta quality and obtain the ETBQZ sets. This also introduces relatively small corrections. The differences between ETBQZ and ETB0 results are smaller than 0.5% of the total values. Therefore, these benchmark results show that the ETB0 sets have sufficient flexibility to provide reliable W_{NSM} values.

As expected, electron correlation makes important contributions to the W_{NSM} values. As shown in Table 1, the electron-correlation contributions at the CCSD level amount to

Table 1: Computed W_{NSM} values (a.u.) using the X2CAMF scheme to treat relativistic effects. Enclosed in the parentheses are the electron-correlation contributions at the CCSD level, namely, the differences between CCSD and HF results.

	FrLi		RaF		ThO ($\mathrm{H}^3\Delta_1$)	
	HF	CCSD	HF	CCSD	HF	CCSD
ETB0	-25006	-23063	-23147	-20254	-32243	-25772
		(1943)		(2893)		(6471)
ETB0+3SP	-25068	-23123	-23153	-20258	-32356	-25881
		(1945)		(2895)		(6475)
ETBSPD	-24968	-23027	-22914	-20027	-31904	-25465
		(1941)		(2887)		(6439)
ETBQZ	-24936	-23079	-23247	-20354	-32368	-25846
		(1857)		(2893)		(6422)

around 8%, 14%, and 25% of the total W_{NSM} values in FrLi, RaF, and ThO, respectively. It is thus necessary to include electron-correlation contributions to obtain accurate W_{NSM} values. Relativistic coupled-cluster methods provide robust treatments of electron correlation and are methods of choice for reliable prediction of W_{NSM} values. Meanwhile, we note that the HF calculations can provide qualitatively correct results that serve as useful initial estimates for the magnitudes of the W_{NSM} values. Based on the present CC results, we find that relativistic density-functional theory calculations[11] provide reasonably good W_{NSM} values.

Table 2 provides a comparison of W_{NSM} values computed in the present study to available calculations in the literature. The present results for AcF, AcN, AcO$^+$, EuO$^+$, EuN, and TlF are around 20% smaller than the values reported in Ref. 13. The only major discrepancy that we observe is that the present results for the $^1\Sigma^+$ state of ThO are significantly smaller than those reported in Ref. 13. For example, the present X2CAMF-HF value of -4351 a.u. is an order of magnitude smaller than the HF value of -20333 a.u. in Ref. 13. We performed a HF calculation using the X2CAMF(DC) scheme and obtained a value of -4621 a.u.. This X2CAMF(DC)-HF value agrees well with a value of -4814 a.u. obtained from four-component DC-HF calculations by Skripnikov and collaborators.[195] The discrepancy between these results from all-electron relativistic two- and four-component calculations and the

Table 2: Computed W_{NSM} values (a.u.) for the closed-shell electronic ground states of heavy-atom-containing molecules using the X2CAMF scheme to treat relativistic effects. The ETB0 basis sets were used for the active atoms (Ac, Eu, Tl, Fr, Ra). The uncontracted aug-cc-pVTZ basis sets were used for the light atoms (F, N, O, S, H), and the uncontracted ANO-RCC basis set was used for Ag.

	HF	CCSD	CCSD(T)	Literature
AcF	-9787	-7573	-7399	-8240[13]
AcN	-44577	-38874	-37136	-46295[13]
AcO$^+$	-57778	-48857	-46936	-58461[13]
ThO	-4351	-1684	-2330	-17085[13]
EuO$^+$	-10775	-9199	-9145	-11677[13]
EuN	-7300	-7086	-7280	-10419[13]
TlF	45021	35319	33279	37192[13]/41136[14]/39967[15]
FrAg	-30815	-29370	-28737	-30168[16]
RaO	-57413	-46878	-43994	-45192[12]
RaSH$^+$	-48451	-44220	-43327	-45060[11]

results in Ref. 13 obtained from a two-step scheme is thus attributed to the approximations in the two-step scheme. We refer the readers to a forthcoming publication of Skripnikov and collaborators for the four-component calculations and analysis of the performance of the two-step scheme.[195]

The present results for RaSH$^+$ and RaO agree well with available relativistic coupled-cluster calculations,[11,12] with discrepancies below 4% of total values. The present results for FrAg also agree well with recent relativistic HF and MRCI calculations.[16] Here the HF value of -30815 a.u. in the present calculation differs from the HF value of -31350 a.u. reported in Ref.[16] by around 500 a.u., less than 2% of the total value. The difference between the electron-correlation contributions amounts to around 800 a.u., which can be attributed to the difference of CC and MRCI in treating electron correlation.

Chemical Mechanisms Contributing to W_{NSM}

A W_{NSM} value is proportional to the gradient of the effective electron density at the position of the active nucleus. It has been pointed out in Ref. 13 that the electron-density gradient at the

position of a heavy atom may have two competing contributions. The electronegative ligand draws electron density from the heavy atom toward the ligand. Meanwhile, the net negative charge in the ligand tends to push the electron density at the heavy atom away from the ligand. Here we specify these two competing types of contributions based on simple chemical concepts. The first one is readily attributed to polar covalent chemical bonds between the heavy metal and an electronegative neighboring atom or functional group. In all of the calculations presented here, the coordinate of the active nucleus along the molecular axis assumes positive values. The polar covalent chemical bonds draw electron density toward the inter-atomic bonding region and thus makes a contribution with a negative sign to W_{NSM}. The second contribution can be attributed to the back-polarization of non-bonding orbitals of the heavy atom, especially the non-bonding valence s-type orbitals, due to the ligand field. This back-polarization of s-type orbitals creates an electron-density deficiency in the inter-atomic bonding region and makes a contribution with a positive sign to W_{NSM}.

We plot the relevant polarized molecular orbitals to illustrate the first mechanism. As shown in Figure 1, a polar molecular orbital in TlF represents a typical σ bonding orbital involving Tl $6s$ (28%), Tl $6p$ (2%), Tl $5d$ (3%), and F $2p$ (67%) contributions. A polar molecular orbital in AcF that makes a significant negative contribution to the NSM value involves Ac $7p$ (12%), Ac $6d$ (6%) and F $2p$ (78%) contributions. These orbitals draw electron densities toward the more electronegative fluorine atom. The present illustration is based on Hartree-Fock orbitals. It might be of interest for future work to perform bond analysis for these molecules and study the relevance of covalency in the bonding to the NSM sensitivity parameters. The second mechanism may not be as well known as the first one, while it can be illustrated well using the back-polarized non-bonding orbitals. The back-polarized Ac $7s$ orbitals in AcF and Tl $6s$ orbitals in TlF are plotted in Figure 1. They lead to an electron density deficiency in the inter-atomic region and contribute significant positive values to the NSM sensitivity parameters. We mention that molecular electric dipole moment values also have these two competing types of contributions. This has been demonstrated, for example,

16

in joint experimental-computational work on thorium halides[196] and in the computational study in Ref. 13.
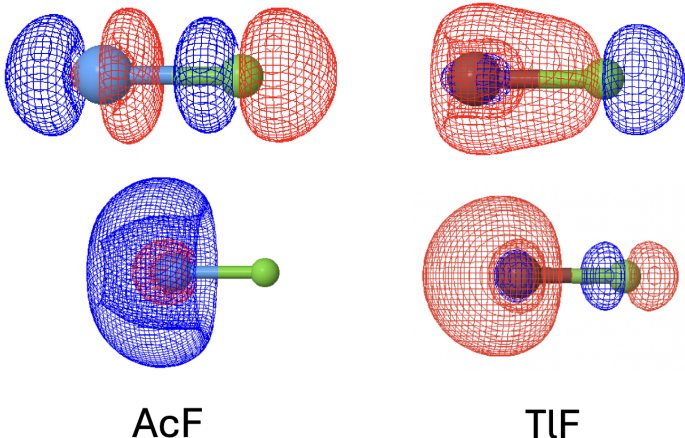

AcF   TlF

Figure 1: The polar orbitals in AcF and TlF (top) that make significant negative contributions to NSM sensitivity parameters and back-polarized Ac $7s$ orbital in AcF and Tl $6s$ orbital in TlF (bottom) that make positive contributions. Isosurfaces with an isovalue of 0.04 for the absolute value of the wave function are plotted. The red and blue colors represent opposite signs of the wave function values.

The relative magnitudes of the W_{NSM} values in AcF, AcN, and AcO$^+$ can be explained using these two mechanisms. The relatively small absolute magnitude of W_{NSM} in AcF comes from a major cancellation between these two contributions. Each electron in the bonding orbital shown in Figure 1 contributes a value of -22095 a.u. to the NSM value. The two non-bonding Ac $7s$ electrons are significantly back-polarized. Each of them contributes a value of 14085 a.u. to W_{NSM} at the HF level. In contrast, AcN and AcO$^+$ have no non-bonding Ac $7s$ electrons. The contributions from back-polarized Ac $7s$ electrons in AcF thus are responsible for most of the differences between the W_{NSM} value in AcF and those in AcN and AcO$^+$.

Interestingly, TlF is an example for particularly significant back-polarization of valence s-type orbitals, as shown in Figure 1. Each back-polarized $6s$ electron of Tl contributes a

value of as large as 32655 a.u. to W_{NSM}. Furthermore, the difference in electronegativity between Tl and F is not as large as that between Ac and F in AcF; the contributions from the first mechanism due to polar covalent chemical bonds is relatively small in TlF. The bonding orbital shown in Figure 1 contributes only -12583 a.u. to the NSM value. These together lead to a W_{NSM} value of a peculiar positive sign in TlF.

In summary, from the perspective of rational design, an ideal NSM-sensitive species would maximize the gradient of electron density at the heavy (ideally octupole-deformed) nucleus, which is achievable in a number of ways. One option is to select molecules with an electronegative ligand that withdraws electron density from the heavy nucleus, maximizing the (negative) contribution due to the polar covalent bond. This can be achieved in molecules with large electronegativity differences between the bonded atoms, and in cases where the heavy atom has empty non-bonding orbitals. Another option would be to select molecules with significant back-polarization of orbitals centered on the heavy atom, increasing the (positive) contribution to W_{NSM}. This can be achieved by selecting bonding partners with similar electronegativities, and doubly occupied non-bonding orbitals that undergo significant back-polarization. Competition between these two effects can lead to values of W_{NSM} with reduced magnitude. In the following we present computed NSM sensitivity factors for thorium-, radium-, and dysprosium-containing molecules, together with analysis of the computational results based on these chemical concepts.

$W_{\mathbf{NSM}}$ values in ThO and ThF$^+$

ThO and ThF$^+$ are already important molecules in the search for the eEDM. The work on precision measurement of ThO by the ACME collaboration has improved the upper bound for the eEDM value by two orders of magnitude compared to earlier records.[101,102] Ongoing and future measurements seek to further improve the sensitivity to the eEDM.[106,109] ThF$^+$ is the molecule of choice for the third-generation JILA eEDM measurement.[107,197] Because the $^3\Delta_1$ state of ThF$^+$ has significantly longer coherence time and larger effective electric field

than that of HfF$^+$, a precision measurement using ThF$^+$ has the potential to improve the current leading sensitivity to the eEDM set with HfF$^+$.[103,104] These molecules are potential candidates for NSM searches, since ^{227}Th and ^{229}Th have been proposed to have octupole deformation.[198–202] Therefore, it is of interest to investigate the possibility of using these molecules in the search for NSMs.
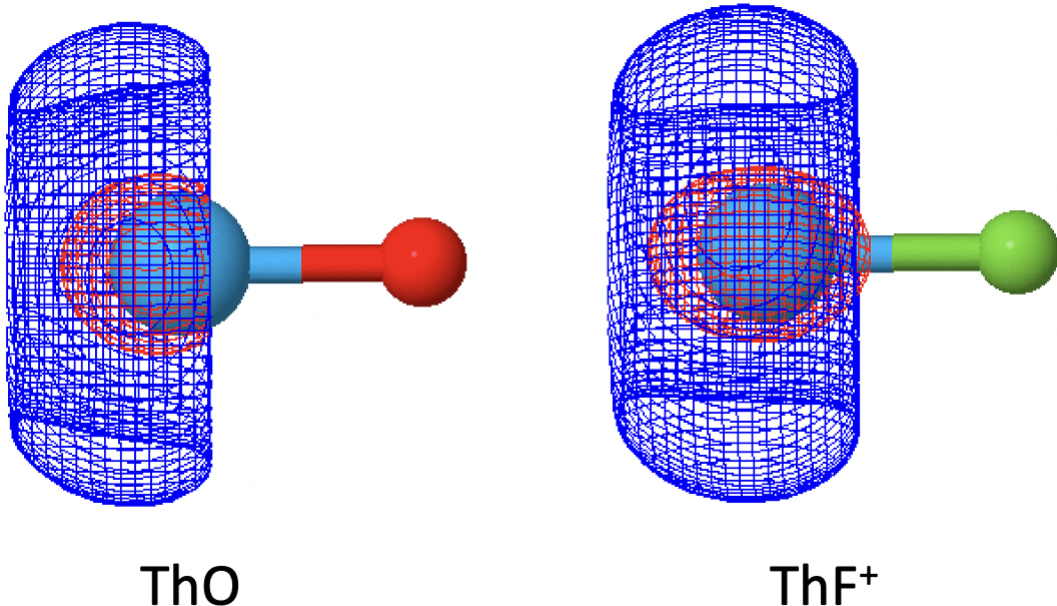

ThO   ThF$^+$

Figure 2: Back-polarized Th $7s$ orbital in the $^1\Sigma^+$ states of ThO and ThF$^+$. Isosurfaces with an isovalue of 0.04 for the absolute value of the wave function are plotted. The red and blue colors represent opposite signs of the wave function values.

The lowest-lying electronic states in both ThO and ThF$^+$ are a closed-shell $^1\Sigma^+$ state (with Th electron configuration $7s^2$) and an open-shell $^3\Delta_1$ state ($7s^16d^1$). In ThO, the $^1\Sigma^+$ state is the ground state, and the $^3\Delta_1$ state is a metastable excited state. By contrast, ThF$^+$ has a $^3\Delta_1$ ground state, while the $^1\Sigma^+$ state is located approximately 500 cm^{-1} higher in energy. The computed W_{NSM} values for both $^1\Sigma^+$ and $^3\Delta_1$ states of ThO and ThF$^+$ are summarized in Table 3. ThO and ThF$^+$ have highly polarized chemical bonds drawing electron densities from Th toward O or F; all computed W_{NSM} values take negative values.

Th $7s$ orbitals are back-polarized by F^- or O^{2-}; Th $7s$ electrons contribute positive values to W_{NSM} that partially cancel the contributions from the polarized chemical bonds. Since a $^1\Sigma^+$ state has one more Th $7s$ electron than a $^3\Delta_1$ state, the W_{NSM} values for the $^1\Sigma^+$ states take smaller absolute values than those of the $^3\Delta_1$ states. As shown in Figure 2, O^{2-} back-polarizes the Th $7s$ orbital more effectively than F^-. The W_{NSM} values in ThO thus show more pronounced cancellation and take smaller absolute values than the corresponding W_{NSM} values in ThF^+. In particular, the $^1\Sigma^+$ state of ThO has two heavily back-polarized Th $7s$ electrons and thus exhibits a W_{NSM} value significantly smaller than the other states.

Table 3: Computed W_{NSM} values using the X2CAMF scheme to treat relativistic effects. The ETB0 basis sets were used for Th and Ra. The uncontracted aug-cc-pVTZ basis sets for H, C, O, F were used in all calculations except that the calculations of $RaCH_3^+$, $RaOCH_3^+$, $RaCH_3$, and $RaOCH_3$ used the SFX2C-1e recontracted cc-pVTZ sets for O, C, and H. The increments with respect to the preceding column are enclosed in the parentheses.

	HF	CCSD	CCSD(T)
DyF ($Dy4f^96s^2$)	-2578	-2113 (465)	-2004 (108)
DyO ($Dy4f^96s^1$)	-9460	-7821 (1638)	-7431 (390)
ThO ($X^1\Sigma^+$)	-4351	-1684 (2667)	-2330 (-646)
ThO ($H^3\Delta_1$)	-33176	-26576 (6600)	-25384 (1192)
ThF^+ ($a^1\Sigma^+$)	-25145	-29811 (-4666)	-31460 (-1649)
ThF^+ ($X^3\Delta_1$)	-44988	-39927 (5061)	-38403 (1524)
RaF^+	-50249	-44987 (5262)	-43916 (1071)
$RaOH^+$	-54914	-49355 (5559)	-48336 (1019)
$RaCH_3^+$	-55788	-49954 (5834)	-48636 (1318)
$RaOCH_3^+$	-55074	-49163 (5911)	-47987 (1176)
RaF	-23147	-20254 (2893)	-19674 (580)
RaOH	-26860	-23397 (3463)	-22877 (520)
$RaCH_3$	-27908	-25202 (2706)	-24695 (507)
$RaOCH_3$	-26552	-23432 (3120)	-22928 (504)

This back-polarization mechanism also explains the relative magnitude of the effective electric fields in the $^3\Delta_1$ states of ThO and ThF^+. The dependence of the effective electric field on $s-p$ mixing is directly analogous to the dependence of W_{NSM} on the electron density gradient near the nucleus. As mentioned above, the Th $7s$ orbital in ThO is back-polarized more significantly than that in ThF^+ and has more contributions from the atomic

Th $7p$ orbitals. An inspection of the molecular spinor compositions shows that the back-polarized "Th $7s$" orbitals in ThO and ThF$^+$ have 7% and 2.5% "Th $7p$" contributions, respectively. The back-polarized Th $7s$ electron in the $^3\Delta_1$ state of ThO thus makes a larger contribution to the effective electric field than that in ThF$^+$, and the effective electric field in ThO is consequently larger than that in ThF$^+$. Note that while the effective electric field depends only on the open-shell electron(s), the NSM sensitivity factors have contributions from all electrons. While the back-polarized Th $7s$ electron in ThO also makes a larger contribution in terms of absolute magnitude for the NSM sensitivity factors, it tends to cancel the contributions from polarized chemical bonds. This results in a NSM sensitivity factor in ThO smaller in absolute magnitude than in ThF$^+$.

$W_{\mathbf{NSM}}$ values for radium-containing molecules
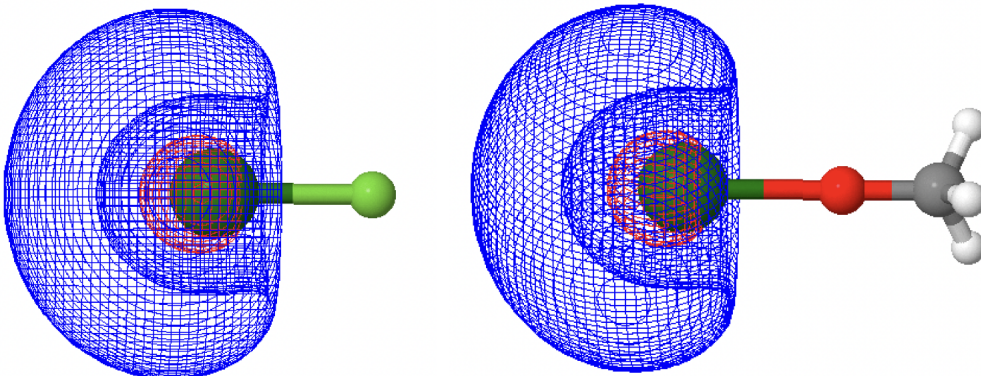
Figure 3: Back-polarized Ra $7s$ orbitals in RaF and RaOCH$_3$. Isosurfaces with an iso-value of 0.04 for the absolute value of the wave function are plotted. The red and blue colors represent opposite signs of the wave function values.

Radium-containing polar molecules have large internal electric fields and hence are expected to have favorable NSM sensitivity parameters. Synthesis, cooling, and trapping of molecular species containing the octupole-deformed ^{225}Ra nucleus[203] thus have the poten-

tial to provide promising platforms for probes of the NSM interaction. Significant progress has recently been reported in this direction.[7] Sympathetic cooling of radium-containing molecular cations[143] and high-resolution laser spectroscopy for a radium-containing neutral molecule, RaF,[204] have been reported. Spectroscopic measurements and relativistic electronic-structure calculations also support the laser-coolability of RaF and RaOH.[205–209,209] Relativistic electronic-structure calculations have also shown that radium-containing molecules exhibit favorable NSM sensitivity factors.[11,12]

Computational results of relativistic coupled-cluster calculations for a set of radium-containing molecules are summarized in Table 3. All radium-containing molecular cations presented here are closed-shell species with no non-bonding valence electrons located at the radium atom. The W_{NSM} values come entirely from the polar chemical bonds between radium and (pseudo-)halogen ligands. As shown in Table 3, The W_{NSM} parameters of these molecular cations take negative values with large absolute magnitude. The neutral species presented here are all molecular radicals having one unpaired electron occupying a Ra $7s$ orbital, which is significantly back-polarized by the ligand, as shown in Figure 3. While this property is favorable for laser cooling, the W_{NSM} contribution from the unpaired electron in the back-polarized orbital tends to cancel the contribution from the polar chemical bonds. Therefore, the W_{NSM} parameters in these neutral molecules are smaller than those in the cations in terms of absolute magnitude, by roughly a factor of two. Nevertheless, all radium-containing molecular species studied here exhibit significant molecular sensitivity factors for the NSM interaction; they are promising candidate molecules for precision measurement probes of BSM physics in the hadronic sector and the strong CP problem.

W_{NSM} values for Dy-containing molecules

Notable nuclei with non-zero octupole deformation parameters, $\langle \beta_3 \rangle \neq 0$, are believed to exist only in radioactive atoms such as Rn–Pu.[119] However, certain lanthanide nuclei also exhibit a dynamical, vibration-like octupole deformation such that $\langle \beta_3^2 \rangle \neq 0$. Since the

enhanced NSM depends quadratically[138] on the deformation parameter, $S \propto \beta_3^2$, these dynamically deformed species may also offer the possibility of highly sensitive measurements. For example, experiments using stable, dynamically octupole-deformed ^{153}Eu^{3+} ions embedded in a crystal are under development, with anticipated sensitivity to CP-violating physics several orders of magnitude beyond current bounds.[210,211] Octupole deformation in Dy has also been established by thorough experimental and theoretical studies,[212] and the stable and naturally abundant ^{161}Dy nucleus is expected to possess a large NSM.[119] Dy-containing piezoelectric solids have already been proposed to probe oscillatory Schiff moments induced by QCD axion dark matter.[213]

Here we consider laser-cooled ^{161}DyO molecules as an intriguing platform for NSM measurements. While a detailed analysis of the laser cooling prospects for DyO is beyond the scope of this work, we briefly explain the potential scheme to motivate the calculation of W_{NSM}. The ground state, X, of DyO has $\Omega = 8$ and is dominated by the Dy$^{2+}[4f^9 6s^1]$O^{2-} configuration. According to ligand field theory calculations, all excited states expected below $\sim$15,000 cm^{-1} have $\Omega < 8$, so that an optical excitation from X to an $\Omega = 9$ state should be electronically closed.[214] The three strongest vibronic bands in the range of 400–700 nm excitation wavelengths are all excitations to $\Omega = 9$ states with rotational constants closely matching that of X.[215] This suggests the possibility of rapid photon cycling on transitions with favorable vibrational branching ratios. A full laser cooling scheme with $\sim$7 lasers—fewer than used to magneto-optically trap CaOH[216]—may be sufficient to close all significant vibrational and rotational loss channels.

Computed values of W_{NSM} DyO and DyF (discussed below) are shown in Table 3. DyO possesses somewhat reduced sensitivity compared to the heavier species considered in this work. For example, W_{NSM} for DyO is only about 30% that of the $^3\Delta_1$ state of ThO, another intrinsically parity-doubled state of a neutral oxide. This is partially explained by the trend that W_{NSM} scales with atomic number generically faster than Z^2, and in addition is consistent with the back-polarization of the dysprosium-centered $6s$ electron. Nevertheless, W_{NSM} is of

the same order of magnitude for DyO as for other species of interest.

To elucidate the effect of back-polarization on W_{NSM} in Dy-containing molecules, we also compute the sensitivity parameter in DyF, which is dominated by a $\mathrm{Dy}^+[4f^9 6s^2]\mathrm{F}^-$ configuration.[217,218] As seen in Table 3, W_{NSM} is nearly a factor of four smaller in DyF than in DyO. This result is explained by the back-polarization of both $6s$ electrons in DyF. Unlike the case of TlF, the combined effect of the back-polarized s electrons does not overwhelm the effect of the bonding mechanism, so that W_{NSM} is reduced in magnitude, but does not adopt a positive sign.

Discussion on the accuracy of the computational results

Let us first analyze the convergence of electron-correlation effects. As shown in Table 3, the triples contributions, i.e., the differences between CCSD(T) and CCSD results, are typically 4-5 times smaller than the singles and doubles contributions. This indicates a nice convergence of the CC series in treating electron-correlation effects on the computed parameters. The triples contributions are smaller than 5% of the total values for all of the systems studied here, except for the $^1\Sigma^+$ state of ThO, in which the total value exhibits a small absolute magnitude because of a major cancellation between the contributions from the two competing mechanisms. The remaining errors in basis sets are no larger than a few percent of the total values, based on the benchmark studies in the previous section. We have also investigated the contributions from the correlation of inner-shell electrons and found that they are also smaller than a few percent of the total values. Therefore, we conclude that the remaining errors in the treatments of electron-correlation and basis-set effects are relatively small.

On the other hand, it is not straightforward to estimate the errors due to the use of approximate nuclear charge distributions. The nuclear charge distributions adopted in the present work consist of single Gaussian functions. These may provide reasonable representations for the overall sizes of the nuclei, but they do not have the correct asymptotic behavior

and do not include detailed information about the nuclear structures. Therefore, it seems logical to expect the computed results to be qualitatively correct, but not quantitatively accurate, despite the fact that the treatments of basis-set and electron-correlation effects have nicely converged.

Summary and Outlook

We report relativistic coupled-cluster calculations of nuclear Schiff moment (NSM) sensitivity factors for molecules containing heavy nuclei, which are promising avenues for searches for physics beyond the Standard Model in the hadronic sector. The use of analytic relativistic coupled-cluster gradient techniques greatly expedites the calculations and enables routine black-box calculations of these parameters. Future work will extend the Cholesky-decomposition-based implementation for exact two-component coupled-cluster methods[93] to analytic gradient calculations, aiming to further improve the computational efficiency by significantly reducing the storage requirement. This will enable routine calculations for molecular sensitivity factors in medium-sized molecules, which might be sufficient to cover the molecular species of interest to the search for the NSM interaction.

We also elucidate two competing chemical mechanisms contributing to the NSM sensitivity factors, one from polar chemical bonds and the other from back-polarization of non-bonding s-type orbitals. We point out simple, chemically-motivated strategies to engineer molecules with large NSM sensitivity factors, by maximizing one of the mechanisms and minimizing the other. TlF illustrated the case in which contributions from back-polarized non-bonding orbitals were maximized, while most of the other species considered relied on highly polar chemical bonds and minimal contributions from back-polarization. While this chemical intuition is a helpful guide, it is in general still necessary to perform first-principle calculations to determine NSM sensitivity factors quantitatively.

Acknowledgments

Supplementary Material

The structures and basis sets used in the calculations.

Declaration of interest statement

The authors report that there are no competing interests to declare.

References

(1) Dine, M.; Kusenko, A. Origin of the matter-antimatter asymmetry. *Reviews of Modern Physics* **2003**, *76*, 1–30.

(2) Kim, J. E.; Carosi, G. Axions and the strong CP problem. *Reviews of Modern Physics* **2010**, *82*, 557–601.

(3) Safronova, M. S.; Budker, D.; DeMille, D.; Kimball, D. F. J.; Derevianko, A.; Clark, C. W. Search for new physics with atoms and molecules. *Rev. Mod. Phys.* **2018**, *90*, 25008.

(4) Hutzler, N. R. Polyatomic molecules as quantum sensors for fundamental physics. *Quantum Science and Technology* **2020**, *5*, 044011.

(5) Alarcon, R. et al. Electric dipole moments and the search for new physics. *arXiv preprint* **2022**, arXiv:2203.08103.

(6) Engel, J.; Ramsey-Musolf, M. J.; van Kolck, U. Electric dipole moments of nucleons, nuclei, and atoms: The Standard Model and beyond. *Progress in Particle and Nuclear Physics* **2013**, *71*, 21–74.

(7) Arrowsmith-Kron, G. et al. Opportunities for Fundamental Physics Research with Radioactive Molecules. *arXiv preprint* **2023**, arXiv:2302.02165.

(8) Gaul, K.; Marquardt, S.; Isaev, T.; Berger, R. Systematic study of relativistic and chemical enhancements of P,T-odd effects in polar diatomic radicals. *Phys. Rev. A* **2019**, *99*, 32509.

(9) Gaul, K.; Berger, R. Ab initio study of parity and time-reversal violation in laser-coolable triatomic molecules. *Phys. Rev. A* **2020**, *101*, 12508.

(10) Gaul, K.; Berger, R. Toolbox approach for quasi-relativistic calculation of molecular properties for precision tests of fundamental physics. *J. Chem. Phys.* **2020**, *152*, 44101.

(11) Gaul, K.; Hutzler, N. R.; Yu, P.; Jayich, A. M.; Iliaš, M.; Borschevsky, A. $\mathcal{CP}$-violation sensitivity of closed-shell radium-containing polyatomic molecular ions. *arXiv preprint* **2023**, arXiv:2312.11687.

(12) Kudashov, A. D.; Petrov, A. N.; Skripnikov, L. V.; Mosyagin, N. S.; Titov, A. V.; Flambaum, V. V. Calculation of the parity- and time-reversal-violating interaction in ^{225}RaO. *Phys. Rev. A* **2013**, *87*, 20102.

(13) Skripnikov, L. V.; Mosyagin, N. S.; Titov, A. V.; Flambaum, V. V. Actinide and lanthanide molecules to search for strong CP-violation. *Phys. Chem. Chem. Phys.* **2020**, *22*, 18374–18380.

(14) Abe, M.; Tsutsui, T.; Ekman, J.; Hada, M.; Das, B. Accurate determination of the enhancement factor X for the nuclear Schiff moment in ^{205}TlF molecule based on the four-component relativistic coupled-cluster theory. *Mol. Phys.* **2020**, *118*, e1767814.

(15) Hubert, M.; Fleig, T. Electric dipole moments generated by nuclear Schiff moment interactions: A reassessment of the atoms ^{129}Xe and ^{199}Hg and the molecule ^{205}TlF. *Phys. Rev. A* **2022**, *106*, 22817.

(16) Marc, A.; Hubert, M.; Fleig, T. Candidate molecules for next-generation searches of hadronic charge-parity violation. *Phys. Rev. A* **2023**, *108*, 62815.

(17) Bartlett, R. J.; Musiał, M. Coupled-cluster theory in quantum chemistry. *Rev. Mod. Phys.* **2007**, *79*, 291–352.

(18) Crawford, T. D.; Schaefer III, H. F. An Introduction to Coupled Cluster Theory for Computational Chemists. *Rev. Comp. Chem.* **2000**, *14*, 33–136.

(19) Purvis III, G. D.; J.Bartlett, R. A full coupled–cluster singles and doubles model: The inclusion of disconnected triples. *J. Chem. Phys.* **1982**, *76*, 1910–1918.

(20) Noga, J.; Bartlett, R. J. The full CCSDT model for molecular electronic structure. *J. Chem. Phys.* **1987**, *86*, 7041–7050.

(21) Scuseria, G. E.; Schaefer III, H. F. A new implementation of the full CCSDT model for molecular electronic structure. *Chem. Phys. Lett.* **1988**, *152*, 382–386.

(22) Watts, J. D.; Bartlett, R. J. The coupled-cluster single, double, and triple excitation model for open-shell single reference functions. *J. Chem. Phys.* **1990**, *93*, 6104.

(23) Oliphant, N.; Adamowicz, L. Coupled-cluster method truncated at quadruples. *J. Chem. Phys.* **1991**, *95*, 6645–6651.

(24) Kucharski, S. A.; Bartlett, R. J. The Coupled-cluster Single, Double, Triple, and Quadruple Excitation Method. *J. Chem. Phys.* **1992**, *97*, 4282–4288.

(25) Kállay, M.; Surján, P. R. Higher excitations in coupled-cluster theory. *J. Chem. Phys.* **2001**, *115*, 2945–2954.

(26) Hirata, S. Tensor Contraction Engine: Abstraction and Automated Parallel Implementation of Configuration-Interaction, Coupled-Cluster, and Many-Body Perturbation Theories. *J. Phys. Chem. A* **2003**, *107*, 9887–9897.

(27) Christiansen, O.; Koch, H.; Jørgensen, P. The second-order approximate coupled cluster singles and doubles model CC2. *Chem. Phys. Lett.* **1995**, *243*, 409–418.

(28) Koch, H.; Christiansen, O.; Jørgensen, P.; Sanchez de Merás, A.; Helgaker, T. The CC3 model: An iterative coupled cluster approach including connected triples. *J. Chem. Phys.* **1997**, *106*, 1808–1818.

(29) Raghavachari, K.; Trucks, G. W.; Pople, J. A.; Head-Gordon, M. A fifth-order perturbation comparison of electron correlation thoeries. *Chem. Phys. Lett.* **1989**, *157*, 479–483.

(30) Bartlett, R. J.; Watts, J. D.; Kucharski, S. A.; Noga, J. Non-iterative fifth-order triple and quadruple excitation energy corrections in correlated methods. *Chem. Phys. Lett.* **1990**, *165*, 513–522.

(31) Stanton, J. F. Why CCSD(T) works: A different perspective. *Chem. Phys. Lett.* **1997**, *281*, 130.

(32) Crawford, T. D.; Stanton, J. F. Investigation of an asymmetric triple-excitation correction for coupled-cluster energies. *Int. J. Quantum Chem.* **1998**, *70*, 601–611.

(33) Kucharski, S. A.; Bartlett, R. J. Noniterative energy corrections through fifth-order to the coupled cluster singles and doubles method. *J. Chem. Phys.* **1998**, *108*, 5243–5254.

(34) Hirata, S.; Nooijen, M.; Grabowski, I.; Bartlett, R. J. Perturbative corrections to coupled-cluster and equation-of-motion coupled-cluster energies: A determinantal analysis. *J. Chem. Phys.* **2001**, *114*, 3919–3928.

(35) Bomble, Y. J.; Stanton, J. F.; Kállay, M.; Gauss, J. Coupled-cluster methods including noniterative corrections for quadruple excitations. *J. Chem. Phys.* **2005**, *123*, 054101.

(36) Kállay, M.; Gauss, J. Approximate treatment of higher excitations in coupled-cluster theory. *J. Chem. Phys.* **2005**, *123*, 214105.

(37) Włoch, M. W.; Piecuch, P. Renormalized coupled-cluster methods exploiting left eigenstates of the similarity-transformed Hamiltonian. *J. Chem. Phys.* **2005**, *123*, 224105.

(38) Włoch, M. W.; Lodriguito, M. D.; Piecuch, P.; Gour, J. R. Two new classes of noniterative coupled-cluster methods derived from the method of moments of coupled-cluster equations. *Mol. Phys.* **2006**, *104*, 2149–2172.

(39) Kállay, M.; Gauss, J. Approximate treatment of higher excitations in coupled-cluster theory. II. Extension to general single-determinant reference functions and improved approaches for the canonical Hartree-Fock case. *J. Chem. Phys.* **2008**, *129*, 144101.

(40) Eriksen, J. J.; Kristensen, K.; Kjærgaard, T.; Jørgensen, P.; Gauss, J. A Lagrangian framework for deriving triples and quadruples corrections to the CCSD energy. *J. Chem. Phys.* **2014**, *140*, 064108.

(41) Eriksen, J. J.; Matthews, D. A.; Jørgensen, P.; Gauss, J. Communication: The Performance of Non-Iterative Coupled Cluster Quadruples Models. *J. Chem. Phys.* **2015**, *143*, 041101.

(42) Adamowicz, L.; Bartlett, R. J. Analytical gradients for the coupled-cluster method. *Int. J. Quantum Chem. Symp.* **1984**, *26*, 245–254.

(43) Scheiner, A. C.; Scuseria, G. E.; Rice, J. E.; Lee, T. J.; Schaefer III, H. F. Analytic evaluation of energy gradients for the single and double excitation coupled cluster (CCSD) wave function: Theory and application. *J. Chem. Phys.* **1987**, *87*, 5361–5373.

(44) Salter, E. A.; Trucks, G. W.; Bartlett, R. J. Analytic energy derivatives in many-body methods. I. First derivatives. *J. Chem. Phys.* **1989**, *90*, 1752–1766.

(45) Salter, E. A.; Bartlett, R. J. Analytic energy derivatives in many-body methods. II. Second derivatives. *J. Chem. Phys.* **1989**, *90*, 1767–1773.

(46) Koch, H.; Jensen, H. J. Aa..; Jørgensen, P.; Helgaker, T.; Scuseria, G. E.; Schaefer III, H. F. Coupled cluster energy derivatives. Analytic Hessian for the closed‚Äêshell coupled cluster singles and doubles wave function: Theory and applications. *J. Chem. Phys.* **1990**, *92*, 4924–4940.

(47) Gauss, J.; Stanton, J. F.; Bartlett, R. J. Coupled-Cluster Open-Shell Analytic Gradients: Implementation of the Direct Product Decomposition Approach in Energy Gradient Calculations. *J. Chem. Phys.* **1991**, *95*, 2623–2638.

(48) Gauss, J.; Stanton, J. F.; Bartlett, R. J. Analytic evaluation of energy gradients at the coupled-cluster singles and doubles level using quasi-restricted Hartree-Fock open,Äêshell reference functions. *J. Chem. Phys.* **1991**, *95*, 2639–2645.

(49) Gauss, J.; Lauderdale, W. J.; Stanton, J. F.; Watts, J. D.; Bartlett, R. J. Analytic energy gradients for open-shell coupled-cluster singles and doubles (CCSD) calculations using restricted open-shell Hartree-Fock (ROHF) reference functions. *Chem. Phys. Lett.* **1991**, *182*, 207–215.

(50) Rendell, A. P.; Lee, T. J. An efficient formulation and implementation of the analytic energy gradient method to the single and double excitation coupled-cluster wave function: Application to Cl_2O_2. *J. Chem. Phys.* **1991**, *94*, 6219–6228.

(51) Scuseria, G. E. Analytic evaluation of energy gradients for the singles and doubles coupled cluster method including perturbative triple excitations: Theory and applications to FOOF and Cr_2. *J. Chem. Phys.* **1991**, *94*, 442–447.

(52) Lee, T. J.; Rendell, A. P. Analytic gradients for coupled-cluster energies that include noniterative connected triple excitations: Application to cis- and trans-HONO. *J. Chem. Phys.* **1991**, *94*, 6229–6236.

(53) Watts, J. D.; Gauss, J.; Bartlett, R. J. Open-shell analytical energy gradients for triple excitation many-body, coupled-cluster methods: MBPT(4), CCSD+T(CCSD), CCSD(T), and QCISD(T). *J. Chem. Phys.* **1992**, *200*, 1–7.

(54) Watts, J. D.; Gauss, J.; Bartlett, R. J. Coupled,Äêcluster methods with noniterative triple excitations for restricted open,Äêshell Hartree,ÄìFock and other general single determinant reference functions. Energies and analytical gradients. *J. Chem. Phys.* **1993**, *98*, 8718–8733.

(55) Gauss, J.; Stanton, J. F. Gauge-invariant calculation of nuclear magnetic shielding

constants at the coupled-cluster singles and doubles level. *J. Chem. Phys.* **1995**, *102*, 251–253.

(56) Gauss, J.; Stanton, J. F. Coupled-cluster calculations of nuclear magnetic resonance chemical shifts. *J. Chem. Phys.* **1995**, *103*, 3561–3578.

(57) Gauss, J.; Stanton, J. F. Analytic CCSD(T) second derivatives. *Chem. Phys. Lett.* **1997**, *276*, 70–77.

(58) Stanton, J. F.; Gauss, J. Analytic second derivatives in high-order many-body perturbation and coupled-cluster theories: Computational considerations and applications. *Int. Rev. Phys. Chem.* **2000**, *19*, 61–95.

(59) Rauhut, G.; Werner, H.-J. Analytical energy gradients for local coupled-cluster methods. *Phys. Chem. Chem. Phys.* **2001**, *3*, 4853–4862.

(60) Gauss, J.; Stanton, J. F. Analytic first and second derivatives for the CCSDT-n (n=1-3) models: a first step towards the efficient calculation of CCSDT properties. *Phys. Chem. Chem. Phys.* **2000**, *2*, 2047–2059.

(61) Gauss, J.; Stanton, J. F. Analytic gradients for the coupled-cluster singles, doubles, and triples (CCSDT) model. *J. Chem. Phys.* **2002**, *116*, 1773–1782.

(62) Gauss, J. Analytic second derivatives for the full coupled-cluster singles, doubles, and triples model: Nuclear magnetic shielding constants for BH, HF, CO, N_2, N_2O, and O_3. *J. Chem. Phys.* **2002**, *116*, 4473–4776.

(63) Kállay, M.; Gauss, J.; Szalay, P. G. Analytic first derivatives for general coupled-cluster and configuration interaction models. *J. Chem. Phys.* **2003**, *119*, 2991–3004.

(64) Kállay, M.; Gauss, J. Analytic second derivatives for general coupled-cluster and configuration-interaction models. *J. Chem. Phys.* **2004**, *120*, 6841–6848.

(65) Bozkaya, U.; Sherrill, C. D. Analytic energy gradients for the coupled-cluster singles and doubles method with the density-fitting approximation. *J. Chem. Phys.* **2016**, *144*, 174103.

(66) Győrffy, W.; Werner, H.-J. Analytical energy gradients for explicitly correlated wave functions. II. Explicitly correlated coupled cluster singles and doubles with perturbative triples corrections: CCSD(T)-F12. *J. Chem. Phys.* **2018**, *148*, 114104.

(67) Feng, X.; Epifanovsky, E.; Gauss, J.; Krylov, A. I. Implementation of analytic gradients for CCSD and EOM-CCSD using Cholesky decomposition of the electron-repulsion integrals and their derivatives: Theory and benchmarks. *J. Chem. Phys.* **2019**, *151*, 014110.

(68) Matthews, D. A. Analytic Gradients of Approximate Coupled Cluster Methods with Quadruple Excitations. *J. Chem. Theory Comput.* **2020**, *16*, 6195–6206.

(69) Schnack-Petersen, A. K.; Koch, H.; Coriani, S.; Kjønstad, E. F. Efficient implementation of molecular CCSD gradients with Cholesky-decomposed electron repulsion integrals. *J. Chem. Phys.* **2022**, *156*, 244111.

(70) Pyykkö, P. Relativistic effects in structural chemistry. *Chem. Rev.* **1988**, *88*, 563–594.

(71) Dyall, K. G.; Fægri Jr, K. *Introduction to relativistic quantum chemistry*; Oxford University Press, 2007.

(72) Autschbach, J. Perspective: relativistic effects. *J. Chem. Phys.* **2012**, *136*, 150902.

(73) Reiher, M.; Wolf, A. *Relativistic quantum chemistry: the fundamental theory of molecular science*; John Wiley & Sons, 2014.

(74) Flambaum, V. Electron electric dipole moment enhancement in heavy atoms. *Yad. Fiz* **1976**, *24*, 383–386, [Sov. J. Nucl. Phys. **1976**, 24, 199].

(75) Sushkov, O.; Flambaum, V. Parity breaking effects in diatomic molecules. *Zh. Eksp. Teor. Fiz* **1978**, *75*, 1208–1213, [Sov. Phys. JETP **1978**, 48, 608].

(76) Sushkov, O.; Flambaum, V.; Khriplovich, I. Possibility of investigating P-and T-odd nuclear forces in atomic and molecular experiments. *Zh. Eksp. Teor. Fiz* **1984**, *87*, 1521, [Sov. Phys. JETP **1984**, 60, 873].

(77) Liu, J.; Cheng, L. Relativistic coupled-cluster and equation-of-motion coupled-cluster methods. *WIREs Comput. Mol. Sci.* **2021**, *11*, e1536.

(78) Kaldor, U.; Heß, B. A. Relativistic all-electron coupled-cluster calculations on the gold atom and gold hydride in the framework of the douglas-kroll transformation. *Chem. Phys. Lett.* **1994**, *230*, 1–7.

(79) Leininger, T.; Nicklass, A.; Stoll, H.; Dolg, M.; Schwerdtfeger, P. The accuracy of the pseudopotential approximation. II. A comparison of various core sizes for indium pseudopotentials in calculations for spectroscopic constants of InH, InF, and InCl. *J. Chem. Phys.* **1996**, *105*, 1052–1059.

(80) Fleig, T.; Visscher, L. Large-scale electron correlation calculations in the framework of the spin-free dirac formalism: the Au_2 molecule revisited. *Chemical Physics* **2005**, *311*, 113.

(81) Cheng, L.; Gauss, J. Analytical evaluation of first-order electrical properties based on the spin-free Dirac-Coulomb Hamiltonian. *J. Chem. Phys.* **2011**, *134*.

(82) Cheng, L.; Gauss, J. Analytic energy gradients for the spin-free exact two-component theory using an exact block diagonalization for the one-electron Dirac Hamiltonian. *J. Chem. Phys.* **2011**, *135*, 084114.

(83) Kirsch, T.; Engel, F.; Gauss, J. Analytic evaluation of first-order properties within the

mean-field variant of spin-free exact two-component theory. *J. Chem. Phys.* **2019**, *150*, 204115.

(84) Visscher, L.; Dyall, K. G.; Lee, T. J. Kramers-restricted closed-shell CCSD theory. *Int. J. Quantum Chem.* **1995**, *56*, 411–419.

(85) Visscher, L.; Lee, T. J.; Dyall, K. G. Formulation and implementation of a relativistic unrestricted coupled-cluster method including noniterative connected triples. *J. Chem. Phys.* **1996**, *105*, 8769–8776.

(86) Lee, H.-S.; Han, Y.-K.; Kim, M. C.; Bae, C.; Lee, Y. S. Spin-orbit effects calculated by two-component coupled-cluster methods: test calculations on AuH, Au_2, TlH and Tl_2. *Chem. Phys. Lett.* **1998**, *293*, 97–102.

(87) Eliav, E.; Kaldor, U.; Hess, B. A. The relativistic Fock-space coupled-cluster method for molecules: CdH and its ions. *J. Chem. Phys.* **1998**, *108*, 3409–3415.

(88) Wang, F.; Gauss, J.; van Wüllen, C. Closed-shell coupled-cluster theory with spin-orbit coupling. *J. Chem. Phys.* **2008**, *129*, 64113.

(89) Wang, F.; Gauss, J. Analytic energy gradients in closed-shell coupled-cluster theory with spin-orbit coupling. *J. Chem. Phys.* **2008**, *129*, 174110.

(90) Nataraj, H. S.; Kállay, M.; Visscher, L. General implementation of the relativistic coupled-cluster method. *J. Chem. Phys.* **2010**, *133*, 234109.

(91) Liu, J.; Shen, Y.; Asthana, A.; Cheng, L. Two-component relativistic coupled-cluster methods using mean-field spin-orbit integrals. *J. Chem. Phys.* **2018**, *148*, 034106.

(92) Pototschnig, J. V.; Papadopoulos, A.; Lyakh, D. I.; Repisky, M.; Halbert, L.; Severo Pereira Gomes, A.; Jensen, H. J. A.; Visscher, L. Implementation of Relativistic Coupled Cluster Theory for Massively Parallel GPU-Accelerated Computing Architectures. *J. Chem. Theory Comput.* **2021**, *17*, 5509–5529.

(93) Zhang, C.; Lipparini, F.; Stopkowicz, S.; Gauss, J.; Cheng, L. Cholesky Decomposition-Based Implementation of Relativistic Two-Component Coupled-Cluster Methods for Medium-Sized Molecules. *J. Chem. Theory Comput.* **2024**, *20*, 787–798.

(94) DeMille, D. Diatomic molecules, a window onto fundamental physics. *Phys. Today* **2015**, *68*, 34–40.

(95) DeMille, D.; Doyle, J. M.; Sushkov, A. O. Probing the frontiers of particle physics with tabletop-scale experiments. *Science (80-.).* **2017**, *357*, 990 LP – 994.

(96) Cairncross, W. B.; Ye, J. Atoms and molecules in the search for time-reversal symmetry violation. *Nat. Rev. Phys.* **2019**, *1*, 510–521.

(97) Sandars, P. G. H. The electric dipole moment of an atom. *Phys. Lett.* **1965**, *14*, 194.

(98) Sandars, P. G. H. Measurability of the Proton Electric Dipole Moment. *Phys. Rev. Lett.* **1967**, *19*, 1396–1398.

(99) Hudson, J. J.; Sauer, B. E.; Tarbutt, M. R.; Hinds, E. A. Measurement of the Electron Electric Dipole Moment Using YbF Molecules. *Phys. Rev. Lett.* **2002**, *89*, 23003.

(100) Hudson, J. J.; Kara, D. M.; Smallman, I. J.; Sauer, B. E.; Tarbutt, M. R.; Hinds, E. A. Improved measurement of the shape of the electron. *Nature* **2011**, *473*, 493–496.

(101) Baron, J. et al. Order of Magnitude Smaller Limit on the Electric Dipole Moment of the Electron. *Science (80-.).* **2014**, *343*, 269 LP – 272.

(102) Andreev, V.; Ang, D. G.; DeMille, D.; Doyle, J. M.; Gabrielse, G.; Haefner, J.; Hutzler, N. R.; Lasner, Z.; Meisenhelder, C.; O'Leary, B. R.; Panda, C. D.; West, A. D.; West, E. P.; Wu, X.; Collaboration, A. Improved limit on the electric dipole moment of the electron. *Nature* **2018**, *562*, 355–360.

(103) Cairncross, W. B.; Gresh, D. N.; Grau, M.; Cossel, K. C.; Roussy, T. S.; Ni, Y.; Zhou, Y.; Ye, J.; Cornell, E. A. Precision Measurement of the Electron's Electric Dipole Moment Using Trapped Molecular Ions. *Phys. Rev. Lett.* **2017**, *119*, 153001.

(104) Roussy, T. S.; Caldwell, L.; Wright, T.; Cairncross, W. B.; Shagam, Y.; Ng, K. B.; Schlossberger, N.; Park, S. Y.; Wang, A.; Ye, J.; Cornell, E. A. An improved bound on the electron's electric dipole moment. *Science (80-.).* **2023**, *381*, 46–50.

(105) Regan, B. C.; Commins, E. D.; Schmidt, C. J.; DeMille, D. New Limit on the Electron Electric Dipole Moment. *Phys. Rev. Lett.* **2002**, *88*, 71805.

(106) Wu, X.; Han, Z.; Chow, J.; Ang, D. G.; Meisenhelder, C.; Panda, C. D.; West, E. P.; Gabrielse, G.; Doyle, J. M.; DeMille, D. The metastable Q3Δ2 state of ThO: a new resource for the ACME electron EDM search. *New J. Phys.* **2020**, *22*, 23013.

(107) Ng, K. B.; Zhou, Y.; Cheng, L.; Schlossberger, N.; Park, S. Y.; Roussy, T. S.; Caldwell, L.; Shagam, Y.; Vigil, A. J.; Cornell, E. A.; Ye, J. Spectroscopy on the electron-electric-dipole-moment–sensitive states of ThF$^+$. *Phys. Rev. A* **2022**, *105*, 22823.

(108) Zhang, C.; Zhang, C.; Cheng, L.; Steimle, T. C.; Tarbutt, M. R. Inner-shell excitation in the YbF molecule and its impact on laser cooling. *J. Mol. Spectrosc.* **2022**, *386*, 111625.

(109) Hiramoto, A.; Masuda, T.; Ang, D. G.; Meisenhelder, C.; Panda, C.; Sasao, N.; Uetake, S.; Wu, X.; Demille, D.; Doyle, J. M.; Gabrielse, G.; Yoshimura, K. SiPM module for the ACME III electron EDM search. *Nucl. Instruments Methods Phys. Res. Sect. A Accel. Spectrometers, Detect. Assoc. Equip.* **2023**, *1045*, 167513.

(110) Popa, S.; Schaller, S.; Fielicke, A.; Lim, J.; Sartakov, B. G.; Tarbutt, M. R.; Meijer, G. Understanding inner-shell excitations in molecules through spectroscopy of the 4f hole states of YbF. *arXiv preprint* **2024**, arXiv:2402.10692.

(111) Stadnik, Y. V.; Flambaum, V. V. Nuclear spin-dependent interactions: searches for WIMP, axion and topological defect dark matter, and tests of fundamental symmetries. *Eur. Phys. J. C* **2015**, *75*, 110.

(112) Stadnik, Y. V.; Flambaum, V. V. New generation low-energy probes for ultralight axion and scalar dark matter. *Mod. Phys. Lett. A* **2017**, *32*, 1740004.

(113) Stadnik, Y.; Dzuba, V.; Flambaum, V. Improved Limits on Axionlike-Particle-Mediated P, T-Violating Interactions between Electrons and Nucleons from Electric Dipole Moments of Atoms and Molecules. *Phys. Rev. Lett.* **2018**, *120*, 13202.

(114) Flambaum, V.; Pospelov, M.; Ritz, A.; Stadnik, Y. Sensitivity of EDM experiments in paramagnetic atoms and molecules to hadronic CP violation. *Phys. Rev. D* **2020**, *102*, 35001.

(115) Flambaum, V.; Samsonov, I.; Tran Tan, H. Effects of CP-violating internucleon interactions in paramagnetic molecules. *Phys. Rev. D* **2020**, *102*, 115036.

(116) Flambaum, V. V.; Samsonov, I. B.; Tran Tan, H. B. Limits on CP-violating hadronic interactions and proton EDM from paramagnetic molecules. *J. High Energy Phys.* **2020**, *2020*, 77.

(117) Maison, D. E.; Flambaum, V. V.; Hutzler, N. R.; Skripnikov, L. V. Electronic structure of the ytterbium monohydroxide molecule to search for axionlike particles. *Phys. Rev. A* **2021**, *103*, 22813.

(118) Roussy, T. S.; Palken, D. A.; Cairncross, W. B.; Brubaker, B. M.; Gresh, D. N.; Grau, M.; Cossel, K. C.; Ng, K. B.; Shagam, Y.; Zhou, Y.; Flambaum, V. V.; Lehnert, K. W.; Ye, J.; Cornell, E. A. Experimental Constraint on Axionlike Particles over Seven Orders of Magnitude in Mass. *Phys. Rev. Lett.* **2021**, *126*, 171301.

(119) Dalton, F.; Flambaum, V. V.; Mansour, A. J. Enhanced Schiff and magnetic quadrupole moments in deformed nuclei and their connection to the search for axion dark matter. *Physical Review C* **2023**, *107*, 035502.

(120) Ginges, J. S. M.; Flambaum, V. V. Violations of fundamental symmetries in atoms and tests of unification theories of elementary particles. *Phys. Rep.* **2004**, *397*, 63–154.

(121) Johnson, W. R.; Guo, D. S.; Idrees, M.; Sapirstein, J. Weak-interaction effects in heavy atomic systems. II. *Phys. Rev. A* **1986**, *34*, 1043–1057.

(122) Cossel, K. C.; Gresh, D. N.; Sinclair, L. C.; Coffey, T.; Skripnikov, L. V.; Petrov, A. N.; Mosyagin, N. S.; Titov, A. V.; Field, R. W.; Meyer, E. R.; Cornell, E. A.; Ye, J. Broadband velocity modulation spectroscopy of HfF^+: Towards a measurement of the electron electric dipole moment. *Chem. Phys. Lett.* **2012**, *546*, 1–11.

(123) Skripnikov, L. V.; Petrov, A. N.; Titov, A. V. Communication: Theoretical study of ThO for the electron electric dipole moment search. *J. Chem. Phys.* **2013**, *139*, 221103.

(124) Petrov, A. N.; Skripnikov, L. V.; Titov, A. V.; Hutzler, N. R.; Hess, P. W.; O'Leary, B. R.; Spaun, B.; DeMille, D.; Gabrielse, G.; Doyle, J. M. Zeeman interaction in ThO for the electron electric-dipole-moment search. *Phys. Rev. A* **2014**, *89*, 62505.

(125) Fleig, T.; Nayak, M. K. Electron electric dipole moment and hyperfine interaction constants for ThO. *J. Mol. Spectrosc.* **2014**, *300*, 16–21.

(126) Denis, M.; Nørby, M. S.; Jensen, H. J. A.; Gomes, A. S. P.; Nayak, M. K.; Knecht, S.; Fleig, T. Theoretical study on ThF^+, a prospective system in search of time-reversal violation. *New J. Phys.* **2015**, *17*, 43005.

(127) Skripnikov, L. V.; Titov, A. V. Theoretical study of thorium monoxide for the electron electric dipole moment search: Electronic properties of $H^3\Delta_1$ in ThO. *J. Chem. Phys.* **2015**, *142*, 024301.

(128) Skripnikov, L. V. Combined 4-component and relativistic pseudopotential study of ThO for the electron electric dipole moment search. *J. Chem. Phys.* **2016**, *145*, 214301.

(129) Skripnikov, L. V. Communication: Theoretical study of HfF^+ cation to search for the T,P-odd interactions. *J. Chem. Phys.* **2017**, *147*, 021101.

(130) Fleig, T. P, T-odd and magnetic hyperfine-interaction constants and excited-state lifetime for HfF^+. *Phys. Rev. A* **2017**, *96*, 40502.

(131) Fleig, T.; DeMille, D. Theoretical aspects of radium-containing molecules amenable to assembly from laser-cooled atoms for new physics searches. *New J. Phys.* **2021**, *23*, 113039.

(132) Flambaum, V. V.; Dzuba, V. A. Electric dipole moments of atoms and molecules produced by enhanced nuclear Schiff moments. *Physical Review A* **2020**, *101*, 42504.

(133) Flambaum, V. V.; Demille, D.; Kozlov, M. G. Time-Reversal Symmetry Violation in Molecules Induced by Nuclear Magnetic Quadrupole Moments. *Physical Review Letters* **2014**, *113*, 103003.

(134) Flambaum, V. V.; Khriplovich, I. B.; Sushkov, O. P. On the P- and T-nonconserving nuclear moments. *Nuclear Physics A* **1986**, *449*, 750–760.

(135) Flambaum, V. V. Spin hedgehog and collective magnetic quadrupole moments induced by parity and time invariance violating interaction. *Physics Letters B* **1994**, *320*.

(136) Lackenby, B. G. C.; Flambaum, V. V. Time reversal violating magnetic quadrupole moment in heavy deformed nuclei. *Physical Review D* **2019**, *98*.

(137) Flambaum, V. V.; Mansour, A. J. Enhanced magnetic quadrupole moments in nuclei with octupole deformation and their CP-violating effects in molecules. *Physical Review C* **2022**, *105*, 65503.

(138) Spevak, V.; Auerbach, N.; Flambaum, V. V. Enhanced T-odd, P-odd electromagnetic moments in reflection asymmetric nuclei. *Physical Review C* **1997**, *56*, 1357.

(139) Haxton, W. C.; Henley, E. M. Enhanced T-Nonconserving Nuclear Moments. *Physical Review Letters* **1983**, *51*, 1937.

(140) Stadnik, Y.; Flambaum, V. Axion-induced effects in atoms, molecules, and nuclei: Parity nonconservation, anapole moments, electric dipole moments, and spin-gravity and spin-axion momentum couplings. *Phys. Rev. D* **2014**, *89*, 43522.

(141) Abel, C. et al. Search for Axionlike Dark Matter through Nuclear Spin Precession in Electric and Magnetic Fields. *Phys. Rev. X* **2017**, *7*, 41034.

(142) Aybas, D. et al. Search for Axionlike Dark Matter Using Solid-State Nuclear Magnetic Resonance. *Phys. Rev. Lett.* **2021**, *126*, 141802.

(143) Fan, M.; Holliman, C.; Shi, X.; Zhang, H.; Straus, M.; Li, X.; Buechele, S.; Jayich, A. Optical Mass Spectrometry of Cold RaOH and $RaOCH_3^+$. *Phys. Rev. Lett.* **2021**, *126*, 23002.

(144) Kłos, J.; Li, H.; Tiesinga, E.; Kotochigova, S. Prospects for assembling ultracold radioactive molecules from laser-cooled atoms. *New J. Phys.* **2022**, *24*, 25005.

(145) Yu, P.; Hutzler, N. R. Probing Fundamental Symmetries of Deformed Nuclei in Symmetric Top Molecules. *Physical Review Letters* **2021**, *126*, 023003.

(146) Maison, D.; Skripnikov, L.; Flambaum, V.; Grau, M. Search for CP-violating nuclear magnetic quadrupole moment using the $LuOH^+$ cation. *J. Chem. Phys.* **2020**, *153*, 224302.

(147) Grasdijk, O.; Timgren, O.; Kastelic, J.; Wright, T.; Lamoreaux, S.; DeMille, D.; Wenz, K.; Aitken, M.; Zelevinsky, T.; Winick, T.; Kawall, D. CeNTREX: a new search for time-reversal symmetry violation in the 205Tl nucleus. *Quantum Sci. Technol.* **2021**, *6*, 44007.

(148) Denis, M.; Hao, Y.; Eliav, E.; Hutzler, N. R.; Nayak, M. K.; Timmermans, R. G.; Borschesvky, A. Enhanced P, T -violating nuclear magnetic quadrupole moment effects in laser-coolable molecules. *Journal of Chemical Physics* **2020**, *152*.

(149) Udrescu, S. M. et al. Precision spectroscopy and laser-cooling scheme of a radium-containing molecule. *Nature Physics 2024 20:2* **2024**, *20*, 202–207.

(150) Sahoo, B. K.; Chaudhuri, R.; Das, B. P.; Mukherjee, D. Relativistic Coupled-Cluster Theory of Atomic Parity Nonconservation: Application to ^{137}Ba$^+$. *Phys. Rev. Lett.* **2006**, *96*, 163003.

(151) Fleig, T.; Nayak, M. K. Electron electric-dipole-moment interaction constant for HfF$^+$ from relativistic correlated all-electron theory. *Phys. Rev. A* **2013**, *88*, 32514.

(152) Kudashov, A. D.; Petrov, A. N.; Skripnikov, L. V.; Mosyagin, N. S.; Isaev, T. A.; Berger, R.; Titov, A. V. Ab initio study of radium monofluoride (RaF) as a candidate to search for parity- and time-and-parity–violation effects. *Phys. Rev. A* **2014**, *90*, 52513.

(153) Abe, M.; Gopakumar, G.; Hada, M.; Das, B. P.; Tatewaki, H.; Mukherjee, D. Application of relativistic coupled-cluster theory to the effective electric field in YbF. *Phys. Rev. A* **2014**, *90*, 22501.

(154) Sasmal, S.; Pathak, H.; Nayak, M. K.; Vaval, N.; Pal, S. Calculation of P,T-odd interaction constant of PbF using Z-vector method in the relativistic coupled-cluster framework. *J. Chem. Phys.* **2015**, *143*, 84119.

44

(155) Prasannaa, V. S.; Vutha, A. C.; Abe, M.; Das, B. P. Mercury Monohalides: Suitability for Electron Electric Dipole Moment Searches. *Phys. Rev. Lett.* **2015**, *114*, 183001.

(156) Skripnikov, L. V.; Titov, A. V. Theoretical study of ThF$^+$ in the search for T,P-violation effects: Effective state of a Th atom in ThF$^+$ and ThO compounds. *Phys. Rev. A* **2015**, *91*, 42504.

(157) Skripnikov, L.; Petrov, A.; Mosyagin, N.; Titov, A.; Flambaum, V. TaN molecule as a candidate for the search for a T, P-violating nuclear magnetic quadrupole moment. *Phys. Rev. A* **2015**, *92*, 012521.

(158) Sasmal, S.; Pathak, H.; Nayak, M. K.; Vaval, N.; Pal, S. Relativistic coupled-cluster study of RaF as a candidate for the parity- and time-reversal-violating interaction. *Phys. Rev. A* **2016**, *93*, 62506.

(159) Fleig, T.; Nayak, M. K.; Kozlov, M. G. TaN, a molecular system for probing P, T-violating hadron physics. *Phys. Rev. A* **2016**, *93*, 012505.

(160) Fleig, T. TaO as a candidate molecular ion for searches of physics beyond the standard model. *Phys. Rev. A* **2017**, *95*, 22504.

(161) Sunaga, A.; Abe, M.; Hada, M.; Das, B. P. Analysis of large effective electric fields of weakly polar molecules for electron electric-dipole-moment searches. *Phys. Rev. A* **2017**, *95*, 12502.

(162) Abe, M.; Prasannaa, V. S.; Das, B. P. Application of the finite-field coupled-cluster method to calculate molecular properties relevant to electron electric-dipole-moment searches. *Phys. Rev. A* **2018**, *97*, 32515.

(163) Maison, D. E.; Skripnikov, L. V.; Flambaum, V. V. Theoretical study of ^{173}YbOH to search for the nuclear magnetic quadrupole moment. *Phys. Rev. A* **2019**, *100*, 32514.

(164) Denis, M.; Haase, P. A. B.; Timmermans, R. G. E.; Eliav, E.; Hutzler, N. R.; Borschevsky, A. Enhancement factor for the electric dipole moment of the electron in the BaOH and YbOH molecules. *Phys. Rev. A* **2019**, *99*, 42512.

(165) Prasannaa, V. S.; Shitara, N.; Sakurai, A.; Abe, M.; Das, B. P. Enhanced sensitivity of the electron electric dipole moment from YbOH: The role of theory. *Phys. Rev. A* **2019**, *99*, 62502.

(166) Sunaga, A.; Abe, M.; Hada, M.; Das, B. P. Merits of heavy-heavy diatomic molecules for electron electric-dipole-moment searches. *Phys. Rev. A* **2019**, *99*, 62506.

(167) Fazil, N. M.; Prasannaa, V. S.; Latha, K. V. P.; Abe, M.; Das, B. P. RaH as a potential candidate for electron electric-dipole-moment searches. *Phys. Rev. A* **2019**, *99*, 52502.

(168) Denis, M.; Hao, Y.; Eliav, E.; Hutzler, N. R.; Nayak, M. K.; Timmermans, R. G.; Borschesvky, A. Enhanced P, T-violating nuclear magnetic quadrupole moment effects in laser-coolable molecules. *J. Chem. Phys.* **2020**, *152*, 084303.

(169) Talukdar, K.; Nayak, M. K.; Vaval, N.; Pal, S. Relativistic coupled-cluster study of BaF in search of CP violation. *J. Phys. B At. Mol. Opt. Phys.* **2020**, *53*, 135102.

(170) Talukdar, K.; Nayak, M. K.; Vaval, N.; Pal, S. Electronic structure parameter of nuclear magnetic quadrupole moment interaction in metal monofluorides. *J. Chem. Phys.* **2020**, *153*, 184306.

(171) Haase, P. A. B. et al. Systematic study and uncertainty evaluation of P, T-odd molecular enhancement factors in BaF. *J. Chem. Phys.* **2021**, *155*, 34309.

(172) Zhang, C.; Zheng, X.; Cheng, L. Calculations of time-reversal-symmetry-violation sensitivity parameters based on analytic relativistic coupled-cluster gradient theory. *Phys. Rev. A* **2021**, *104*, 012814.

(173) Zakharova, A.; Petrov, A. P, T-odd effects for the RaOH molecule in the excited vibrational state. *Phys. Rev. A* **2021**, *103*, 32819.

(174) Maison, D. E.; Skripnikov, L. V.; Penyazkov, G.; Grau, M.; Petrov, A. N. T, P-odd effects in the LuOH$^+$ cation. *Phys. Rev. A* **2022**, *106*, 62827.

(175) Chamorro, Y.; Borschevsky, A.; Eliav, E.; Hutzler, N. R.; Hoekstra, S.; Pašteka, L. F. Molecular enhancement factors for P, T-violating eEDM in BaCH$_3$ and YbCH$_3$ symmetric top molecules. *Phys. Rev. A* **2022**, *106*, 52811.

(176) Oleynichenko, A. V.; Skripnikov, L. V.; Zaitsevskii, A. V.; Flambaum, V. V. Laser-coolable AcOH$^+$ ion for CP-violation searches. *Phys. Rev. A* **2022**, *105*, 22825.

(177) Dzuba, V. A.; Flambaum, V. V.; Ginges, J. S. M.; Kozlov, M. G. Electric dipole moments of Hg, Xe, Rn, Ra, Pu, and TlF induced by the nuclear Schiff moment and limits on time-reversal violating interactions. *Phys. Rev. A* **2002**, *66*, 12111.

(178) Liu, J.; Zheng, X.; Asthana, A.; Zhang, C.; Cheng, L. Analytic evaluation of energy first derivatives for spin–orbit coupled-cluster singles and doubles augmented with noniterative triples method: General formulation and an implementation for first-order properties. *J. Chem. Phys.* **2021**, *154*, 064110.

(179) Zheng, X.; Zhang, C.; Liu, J.; Cheng, L. Geometry optimizations with spinor-based relativistic coupled-cluster theory. *J. Chem. Phys.* **2022**, *156*, 151101.

(180) Zhang, C.; Zheng, X.; Liu, J.; Asthana, A.; Cheng, L. Analytic gradients for relativistic exact-two-component equation-of-motion coupled-cluster singles and doubles method. *J. Chem. Phys.* **2023**, *159*, 244113.

(181) Flambaum, V. V.; Ginges, J. S. M. Nuclear Schiff moment and time-invariance violation in atoms. *Phys. Rev. A* **2002**, *65*, 32113.

(182) Filatov, M. On the calculation of Mössbauer isomer shift. *J. Chem. Phys.* **2007**, *127*, 84101.

(183) Knecht, S.; Fux, S.; van Meer, R.; Visscher, L.; Reiher, M.; Saue, T. Mössbauer spectroscopy for heavy elements: a relativistic benchmark study of mercury. *Theor. Chem. Acc.* **2011**, *129*, 631–650.

(184) Matthews, D. A.; Cheng, L.; Harding, M. E.; Lipparini, F.; Stopkowicz, S.; Jagau, T.-C.; Szalay, P. G.; Gauss, J.; Stanton, J. F. Coupled-cluster techniques for computational chemistry: The CFOUR program package. *J. Chem. Phys.* **2020**, *152*, 214108.

(185) Stanton, J. F.; Gauss, J.; Cheng, L.; Harding, M. E.; Matthews, D. A.; Szalay, P. G. CFOUR, Coupled-Cluster techniques for Computational Chemistry, a quantum-chemical program package. With contributions from A.A. Auer, A. Asthana, R.J. Bartlett, U. Benedikt, C. Berger, D.E. Bernholdt, S. Blaschke, Y. J. Bomble, S. Burger, O. Christiansen, D. Datta, F. Engel, R. Faber, J. Greiner, M. Heckert, O. Heun, M. Hilgenberg, C. Huber, T.-C. Jagau, D. Jonsson, J. Jusélius, T. Kirsch, K. Klein, G.M. KopperW.J. Lauderdale, F. Lipparini, J. Liu, T. Metzroth, L.A. Mück, D.P. O'Neill, T. Nottoli, D.R. Price, E. Prochnow, C. Puzzarini, K. Ruud, F. Schiffmann, W. Schwalbach, C. Simmons, S. Stopkowicz, A. Tajti, J. Vázquez, F. Wang, J.D. Watts, C. Zhang, X. Zheng, and the integral packages MOLECULE (J. Almlöf and P.R. Taylor), PROPS (P.R. Taylor), ABACUS (T. Helgaker, H.J. Aa. Jensen, P. Jørgensen, and J. Olsen), and ECP routines by A. V. Mitin and C. van Wüllen. For the current version, see http://www.cfour.de.

(186) Dyall, K. G. Interfacing relativistic and nonrelativistic methods. IV. One- and two-electron scalar approximations. *J. Chem. Phys.* **2001**, *115*, 9136–9143.

(187) Iliaš, M.; Saue, T. An infinite-order two-component relativistic Hamiltonian by a simple one-step transformation. *J. Chem. Phys.* **2007**, *126*, 064102.

(188) Liu, W.; Peng, D. Exact two-component Hamiltonians revisited. *J. Chem. Phys.* **2009**, *131*, 031104.

(189) Heß, B. A.; Marian, C. M.; Wahlgren, U.; Gropen, O. A mean-field spin-orbit method applicable to correlated wavefunctions. *Chem. Phys. Lett.* **1996**, *251*, 365–371.

(190) Liu, J.; Cheng, L. An atomic mean-field spin-orbit approach within exact two-component theory for a non-perturbative treatment of spin-orbit coupling. *J. Chem. Phys.* **2018**, *148*, 144108.

(191) Zhang, C.; Cheng, L. Atomic Mean-Field Approach within Exact Two-Component Theory Based on the Dirac–Coulomb–ÄìBreit Hamiltonian. *J. Phys. Chem. A* **2022**, *126*, 4537–4553.

(192) Visscher, L.; Dyall, K. G. Dirac-Fock atomic electronic structure calculations using different nuclear charge distributions. *At. Data Nucl. Data Tables* **1997**, *67*, 207–224.

(193) Fægri, K. Relativistic Gaussian basis sets for the elements K - Uuo. *Theor. Chem. Acc.* **2001**, *105*, 252–258.

(194) Roos, B. O.; Lindh, R.; Malmqvist, P.-Å.; Veryazov, V.; Widmark, P.-O. New relativistic ANO basis sets for actinide atoms. *Chem. Phys. Lett.* **2005**, *409*, 295–299.

(195) Skripnikov, L. to be published (2004).

(196) Nguyen, D.-T.; Steimle, T.; Linton, C.; Cheng, L. Optical Stark and Zeeman Spectroscopy of Thorium Fluoride (ThF) and Thorium Chloride (ThCl). *J. Phys. Chem. A* **2019**, *123*, 1423–1433.

(197) Gresh, D. N.; Cossel, K. C.; Zhou, Y.; Ye, J.; Cornell, E. A. Broadband velocity modulation spectroscopy of ThF^+ for use in a measurement of the electron electric dipole moment. *J. Mol. Spectrosc.* **2016**, *319*, 1–9.

(198) Liang, C. F.; Paris, P.; Sheline, R. K.; Nosek, D.; Kvasil, J. Level structure and reflection asymmetry in ^{227}Th. *Phys. Rev. C* **1995**, *51*, 1199–1210.

(199) Hammond, N. J. et al. Observation of $K = 1/2$ octupole deformed bands in ^{227}Th. *Phys. Rev. C* **2002**, *65*, 064315.

(200) Ruchowska, E.; Płóciennik, W.; Żylicz, J.; Mach, H.; Kvasil, J.; Algora, A.; Amzal, N.; Bäck, T.; Borge, M.; Boutami, R.; others Nuclear structure of Th 229. *Physical Review C* **2006**, *73*, 044326.

(201) Gulda, K.; Kurcewicz, W.; Aas, A.; Borge, M.; Burke, D.; Fogelberg, B.; Grant, I.; Hagebø, E.; Kaffrell, N.; Kvasil, J.; others The nuclear structure of 229Th. *Nuclear Physics A* **2002**, *703*, 45–69.

(202) Chishti, M.; O'Donnell, D.; Battaglia, G.; Bowry, M.; Jaroszynski, D.; Singh, B. N.; Scheck, M.; Spagnoletti, P.; Smith, J. Direct measurement of the intrinsic electric dipole moment in pear-shaped thorium-228. *Nature Physics* **2020**, *16*, 853–856.

(203) Auerbach, N.; Flambaum, V.; Spevak, V. Collective T-and P-odd electromagnetic moments in nuclei with octupole deformations. *Phys. Rev. Lett.* **1996**, *76*, 4316.

(204) Garcia Ruiz, R. et al. Spectroscopy of short-lived radioactive molecules. *Nature* **2020**, *581*, 396–400.

(205) Isaev, T. A.; Hoekstra, S.; Berger, R. Laser-cooled RaF as a promising candidate to measure molecular parity violation. *Phys. Rev. A* **2010**, *82*, 52521.

(206) Zaitsevskii, A.; Skripnikov, L. V.; Mosyagin, N. S.; Isaev, T.; Berger, R.; Breier, A. A.; Giesen, T. F. Accurate ab initio calculations of RaF electronic structure appeal to more laser-spectroscopical measurements. *J. Chem. Phys.* **2022**, *156*, 44306.

(207) Osika, Y.; Shundalau, M. Fock-space relativistic coupled cluster study on the RaF

molecule promising for the laser cooling. *Spectrochimica Acta Part A: Molecular and Biomolecular Spectroscopy* **2022**, *264*, 120274.

(208) Athanasakis-Kaklamanakis, M. et al. Pinning down electron correlations in RaF via spectroscopy of excited states. *arXiv preprint* **2023**, arXiv:2308.14862.

(209) Zhang, C.; Hutzler, N. R.; Cheng, L. Intensity-Borrowing Mechanisms Pertinent to Laser Cooling of Linear Polyatomic Molecules. *J. Chem. Theory Comput.* **2023**, *19*, 4136–4148.

(210) Ramachandran, H. D.; Vutha, A. C. Nuclear T -violation search using octopole-deformed nuclei in a crystal. *Physical Review A* **2023**, *108*, 012819.

(211) Sushkov, A. O.; Sushkov, O. P.; Yaresko, A. Effective electric field: Quantifying the sensitivity of searches for new P,T-odd physics with $EuCl_3 \cdot 6\ H_2O$. *Phys. Rev. A* **2023**, *107*, 62823.

(212) Rodríguez-Guzmán, R.; Robledo, L. M. Beyond-mean-field description of octupolarity in dysprosium isotopes with the Gogny-D1M energy density functional. *Physical Review C* **2023**, *108*, 024301.

(213) Arvanitaki, A.; Madden, A.; Tilburg, K. V. The Piezoaxionic Effect. *arXiv preprint* **2021**, arXiv:2112.11466v2.

(214) Carette, P.; Hocquet, A. Ligand field calculation of the lower electronic energy levels of the lanthanide monoxides. *Journal of Molecular Spectroscopy* **1988**, *131*, 301–324.

(215) Kaledin, L. A.; Shenyavskaya, E. A. Electronic spectra of TbO, DyO, and HoO. *Journal of Molecular Spectroscopy* **1981**, *90*, 590–591.

(216) Vilas, N. B.; Hallas, C.; Anderegg, L.; Robichaud, P.; Winnicki, A.; Mitra, D.; Doyle, J. M. Magneto-optical trapping and sub-Doppler cooling of a polyatomic molecule. *Nature 2022 606:7912* **2022**, *606*, 70–74.

(217) Yamamoto, S.; Tatewaki, H. Electronic spectra of DyF studied by four-component relativistic configuration interaction methods. *Journal of Chemical Physics* **2015**, *142*.

(218) McCarthy, M. C.; Bloch, J. C.; Field, R. W.; Kaledin, L. A. Laser Spectroscopy of Dysprosium Monofluoride: Ligand Field Assignments of States Belonging to the 4f96s2, 4f106s, and 4f96s6p Superconfigurations. *Journal of Molecular Spectroscopy* **1996**, *179*, 253–262.